ACS OMEGA

Open Access

http://pubs.acs.org/journal/acsodf

Article

Synthesis, Structural Elucidation, *In Silico* and *In Vitro* Studies of New Class of Methylenedioxyphenyl-Based Amide Derivatives as Potential Myeloperoxidase Inhibitors for Cardiovascular Protection

Reshma Rajan, Sambantham Karthikeyan, and Rajagopal Desikan*

Cite This: *ACS Omega* 2024, 9, 7850−7868

Read Online

ACCESS | Metrics & More | Article Recommendations | Supporting Information

ABSTRACT: Novel methylenedioxyphenyl-based amides, especially *N*-(4-methoxybenzyl)-6-nitrobenzo-[1,3]-dioxole-5-carboxamide (MDC) and *N*-(3-acetylphenyl)-6-nitrobenzo-[1,3]-dioxole-5-carboxamide (ADC), potential cardiovascular preventive agents, are successfully synthesized, and their chemical structures are verified by ^{1}H and ^{13}C NMR, Fourier transform infrared (FT-IR), high-resolution mass spectrometry (HRMS), and single-crystal X-ray diffraction (SC-XRD) analyses. Data obtained from SC-XRD reveal that MDC and ADC are both monoclinic molecules with Z = 2 and 4, respectively. From density functional theory (DFT) calculations, 3.54 and 3.96 eV are the energy gaps of the optimized MDC and ADC structures, respectively. MDC and ADC exhibit an electrophilicity index value of more than 1.5 eV, suggesting that they can act as an electrophile, facilitating bond formation with biomolecules. Hirshfeld surface analysis demonstrates that more than 25% of atomic interactions in both MDC and ADC are from H···H interactions. Based on pharmacokinetic predictions, MDC and ADC exhibit drug-like properties, and molecular docking simulations revealed favorable interactions with active site pockets. Both MDC and ADC achieved higher docking scores of −7.74 and −7.79 kcal/mol, respectively, with myeloperoxidase (MPO) protein. From docking results, MPO was found to be most favorable followed by dipeptidyl peptidase-4 (DPP-4) and α-glucosidase (α-GD). Antioxidant, anti-inflammatory, and *in vitro* enzymatic studies of MDC and ADC indicate that MDC is more selective toward MPO and more potent than ADC. The application of MDC to inhibit myeloperoxidase could be ascertained to reduce the cardiovascular risk factor. This can be supported from the results of computational docking (based on hydrogen bonding and docking score), *in vitro* antioxidant and anti-inflammatory properties, and MPO enzymatic inhibition (based on the percentage of inhibition and IC_{50} values).

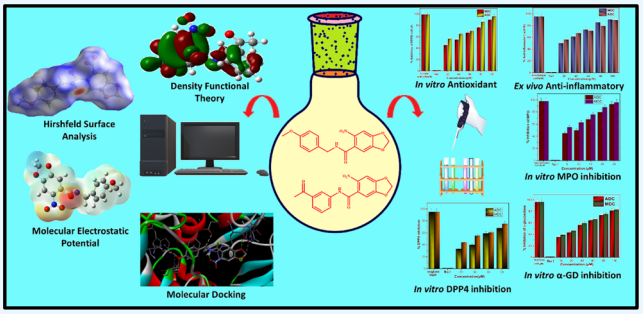

1. INTRODUCTION

A difficult undertaking is the creation of a new drug. Drugs are produced either entirely from natural sources or by semi-synthetic methods. Therapeutic drugs for the treatment of cardiovascular disease (CVD) can be obtained from natural products and their structural equivalents. All social groups are affected by the serious global health problem of CVD. A class of bioactive scaffolds known as substituted methylenedioxyphenyl (MDP) derivatives have been shown to possess antioxidant, antibacterial, antiobesity, antidiabetic, and anti-inflammatory properties.[1−4] The MDP pharmacophore remains of great interest to many research teams as it routinely provides encouraging results for the treatment of CVD.[5−9] A naturally occurring phytochemical derived from *Piper nigrum* (spice bell pepper), piperonylic acid, has MDP pharmacophore. The piperine in *P. nigrum* has been shown to increase the bioavailability of drugs such as resveratrol, quercetin, and nevirapine.[10−12] Potent bioactive drugs in the MDP group that are on the market are shown in Figure 1. Parkinson's disease, diabetes, epilepsy, and urinary tract infections are treated with piribedil, berberine, stiripentol, and cinoxacin, respectively.[13−16] From the reported structure−activity relationship studies, chemical linking of the MDP group to the parent structure appeared to enhance the bioactivity. This is probably due to nucleophilic oxygen in the diether group which readily donates electrons to the electrophilic center for interacting with protein residues within the active site to facilitate biological interactions. Also, the fifth and sixth positions of the MDP group are shown to influence the bioactivity of the molecule.[5,17−19] From the literature, MDP with nitro substitution at the sixth position is shown to offer better cardioprotective effects.[6] Therefore, the nitro group at the sixth

Received: September 29, 2023
Revised: December 18, 2023
Accepted: December 21, 2023
Published: February 7, 2024

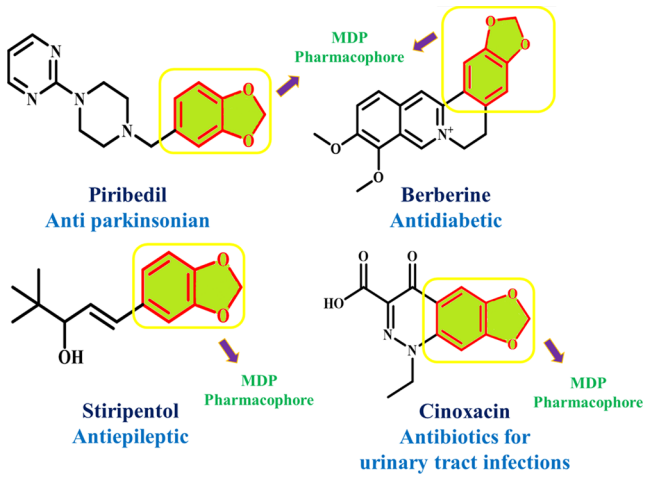

Figure 1. Commercial drugs with methylenedioxyphenyl pharmacophore.

position is kept intact and further modification was done at the fifth position to get better bioactive derivatives.

Methoxy is an essential functional group found in phytochemicals such as curcumin, guaiacol, and methoxyflavone.[20−22] Likewise, the acetophenone group plays a crucial role in the action of numerous medications, including pyrovalerone, amfepramone, and bupropion.[23−25] For the preparation of medications such as zolpidem, oxiconazole, and cinacalcet, basic acetophenone derivatives are used as raw materials.[26] It is therefore anticipated that the combination of 4-methoxybenzylamine, 3-aminoacetophenone, and 6-nitropiperonal (carrying the MDP group) will exhibit significant biological activity. In the present study, a new class of carboxamide derivatives is synthesized with the intention of preserving the pharmacophoric potency of the parent structure and improving the overall bioactivity after creating the amide bond when coupled with piperonylic acid and amines. We first investigated their drug-likeness, molecular docking, and pharmacokinetic properties. The successful results encouraged us to further explore their biological activities, such as antioxidant and anti-inflammatory properties and enzyme inhibitions. α-Glucosidase (α-GD), dipeptidyl peptidase-4 (DPP-4), and myeloperoxidase (MPO) proteins are used for molecular docking. The development of CVD, including atherosclerosis (MPO)[27] and type 2 diabetes (DPP-4[28] and α-GD[29]), is related to these three proteins (MPO, DPP-4, and α-GD). When a macrophage cell dies due to neutrophil extracellular trap (NETosis) activation, chromatin is released into the extracellular environment to trap and eliminate microorganisms. One of the direct links between diabetes and atherosclerosis that can be demonstrated in the inflammatory pathways is NETosis.[30,31] Clinical studies have shown that the link between inflammation, diabetes, and atherosclerosis increases the risk of CVD.[32,33] Therefore, it is essential to look into the anti-inflammatory characteristics of the molecules in relation to CVD. ^{1}H, ^{13}C NMR, Fourier transform infrared (FT-IR), and High-resolution mass spectrometry (HRMS) are used to characterize the synthesized structures. Furthermore, single-crystal X-ray diffraction (SC-XRD) data unequivocally corroborated the molecules' entire chemical structure. To assess the quantum chemical parameters and to expose the crystals' theoretical and experimental bond angles and bond lengths, the Hirshfeld surface analysis is carried out with SC-XRD CIF data. From the Hirshfeld surface analysis, the molecules' volume, asphericity, inner area, d_i, d_e, d_{norm}, and globularity are determined, and their global hardness, global electrophilicity index, dipole moment, global softness, and electron negativity are determined from density functional theory (DFT).

The recently synthesized small molecule drug for MPO inhibition in clinical trials, Verdiperstat, is produced by AstraZeneca and Biohaven Pharmaceuticals. Mild adverse effects including nausea, headache, and insomnia have been linked to verdiperstat.[34,35] Therefore, the appending of a brand-new medication for MPO inhibition that has fewer negative effects is urgently needed. The present study focuses on the synthesis and application of phytochemical-based organic scaffolds targeting cardiovascular disease risk factors, namely, diabetes and atherosclerosis. Sci-Finder search showed limited scientific reports in the literature for nitro-substituted methylenedioxyphenyl amide-based molecules.[36,37] Imidazole, isoindoline, pyridine, triazole, quinoline, and thiosemicarbazone-based heterocyclic derivatives targeting diabetes and atherosclerosis have been reported.[38−43] Relatively, a few phytochemical-based scaffolds are used for treating diabetes and atherosclerosis.[44−46] Chemically linking phytochemical derivatives to organic molecules improves the efficacy and reduces the toxicity of the drug. Thus, minimal toxicity and maximal effectiveness are anticipated when piperine derivatives are chemically linked to an amine via an amide bond. Introducing a novel class of small compounds for MPO inhibition that are inspired by nature is the goal of this endeavor.

2. MATERIALS AND METHODS

Starting materials, deuterated solvents, and reagents are bought from TCI Chemicals, Avra, and Sigma-Aldrich. Solvents are bought from SD Fine Chemicals. ProTox-II predicts molecule toxicity, while SwissADME and pkCSM predict ADME characteristics. Molecular docking is performed using AutoDockTools 1.5.1, and visualizations are performed using Discovery Studio Visualizer v21.1.0.20298. Myeloperoxidase, dipeptidyl peptidase-4, and α-glucosidase are purchased from Sigma-Aldrich.

2.1. Pharmacokinetic Studies. The pharmacokinetic (body action on the drug) features of MDC and ADC are calculated using the free online programs SwissADME, pkCSM, and ProTox-II.[47−49] Toxicological qualities of drugs are predicted using ProTox-II, and SwissADME and pkCSM are used to identify ADME (absorption, distribution, metabolism, and excretion) properties. Clinical trial HITS rejection rates are significantly lowered by ADMET investigations, which have grown to be an essential component in the development of new drugs. Drug-likeness, oral bioavailability, and physicochemical characteristics are all clarified by ADMET.

2.2. Molecular Docking. The binding interactions of hit compounds with targeted proteins are determined using an *in silico* molecular docking (MD) simulation. To ascertain whether ligands and proteins interact well, this method is employed as a reference tool. Three key proteins—myeloperoxidase (MPO), dipeptidyl peptidase-4 (DPP-4), and α-glucosidase (α-GD)—were chosen for MD simulations to examine the binding capacity of MDC and ADC for various disease targets, including atherosclerosis and antidiabetic effects. You can download the crystal structures of the proteins

https://doi.org/10.1021/acsomega.3c07555
ACS Omega 2024, 9, 7850−7868

Scheme 1. Synthesis of MDC and ADC.

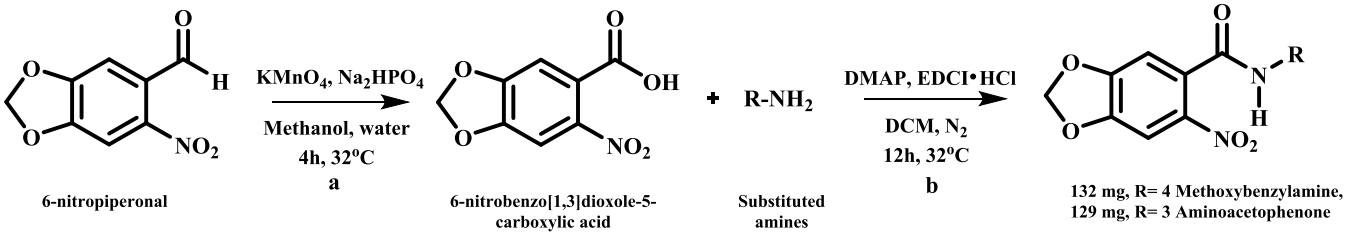

MPO (PDB code 5FIW), DPP-4 (PDB code 6B1E), and α-GD (PDB code 3A4A) from the RCSB Protein Data Bank.[50−52] Salicylhydroxamic acid, sitagliptin, and acarbose are used as positive controls for MPO, DPP-4, and α-GD, respectively. In preparation for docking, the proteins and ligands are created using discovery studio. For docking, AutoDockTool 1.5.6 makes use of the Lamarckian genetic algorithm. Active protein sites are chosen, and a grid box is created to frame all of the active sites before docking.

2.3. Synthesis and Crystallization. The syntheses of MDC and ADC are achieved through two steps. Initially 6-nitropiperonal is oxidized to 6-nitrobenzo[1,3]dioxole-5-carboxylic acid[53] and coupled with 4-methoxybenzylamine/3-aminoacetophenone to form 6-nitrobenzo[1,3]dioxole-5-carboxamide derivatives (Scheme 1). Similar syntheses with different reaction conditions are reported in the literature.[54,55] The method used in this research is well known, simple, and highly useful for researchers to accomplish the synthesis of amide derivatives from aldehydes by using a simple synthetic procedure. The complete methodology is provided in the Supporting Information. The reaction is optimized by changing various experimental parameters like reagents, solvents, and time to achieve a maximum yield with highest purity. When the reaction was conducted in methanol at 32 °C for 4 h with $KMnO_4$ and Na_2HPO_4 as reagents, the maximum yield was achieved (Table 1). Similarly, for step 2, coupling

Table 1. Oxidation of Aldehyde under Different Reaction Conditions[a]

s. no.	oxidizing agent	reagent	solvent	reaction condition	yield (%)
1	MnO_2	$NaHSO_3$	ethanol	12 h, 32 °C	60
2	$KMnO_4$	$NaHSO_3$	methanol	30 min, 32 °C	55
3	$KMnO_4$	Na_2HPO_4	methanol	6 h, 32 °C	75
4	$KMnO_4$	Na_2HPO_4, NH_4Cl	methanol	4 h, 32 °C	81

[a]All reactions were carried out on a 100 mg scale. Aldehyde (1.0 equiv), oxidizing agent (1.0 equiv), reagent (1.0 equiv), and solvent (5 mL). MnO_2: manganese dioxide, $NaHSO_3$: sodium bisulfite, $KMnO_4$: potassium permanganate, Na_2HPO_4: disodium hydrogen phosphate, NH_4Cl: ammonium chloride, h—hour.

agents, bases, and solvents were varied. The maximum yield was obtained when dimethylaminopyridine was used as the base and (3-dimethylamino-propyl)-ethyl-carbodiimide hydrochloride as the coupling agent. The reaction was carried out under an inert atmosphere for 12 h at 32 °C in dichloromethane (Table 2). Dimethyl sulfoxide and hexane (1:1) solvents were used to crystallize MDC and ADC. The crystals were separated, dried, and analyzed for single-crystal X-ray diffraction.

Table 2. Acid Amine Coupling under Different Reaction Conditions[a]

s. no	base	reagents	solvent	reaction condition	yield (%)
1	TEA	EDCI·HCl	DCM	32 °C, 12 h	65
2	DMAP	DCC	DMF	32 °C, 12 h	77
3	DMAP	EDCI·HCl	$CHCl_3$	32 °C, 12 h, N_2	76
4	DMAP	EDCI·HCl	DCM	32 °C, 12 h, N_2	85
5	TEA	DCC	Benzene	32 °C, 12 h, N_2	69

[a]All reactions were carried out on a 100 mg scale. Acid (1.0 equiv), amine (1.0 equiv), base (2.0 equiv), reagent (2.0 equiv), and solvent (10 mL). TEA: triethylamine, EDCI·HCl: (3-dimethylamino-propyl)-ethyl-carbodiimide hydrochloride, DMAP: 4 dimethylaminopyridine, DCC: *N,N′*-dicyclohexylcarbodiimide, h: hour.

2.4. Single-Crystal X-Ray Diffraction Studies. Table 3 summarizes the crystal and structure refinement data for MDC and ADC. The X-ray crystallographic investigation is performed on MDC and ADC with approximate dimensions of 0.098 mm × 0.170 mm × 0.200 mm and 0.120 mm × 0.145 mm × 0.186 mm, respectively. X-ray diffraction intensities are measured on a Bruker D8 Quest with i-mu-s microfocus molybdenum source Mo Kα (λ = 0.71073 Å) radiation. A Bruker SHELXL-2019/1 is used to solve and refine the crystal structure of molecules. The CCDC deposition numbers for single crystals of MDC and ADC are 2239892 and 2282346, respectively.

2.5. Computational Analysis. Quantum chemical computational analysis has advanced significantly in recent years and is now a highly effective method for confirming experimental results. The B3LYP/6-311G** level of theory in the Gaussian-16 program is used to study the quantum chemical parameters. Using DFT, energy calculations of the optimized structures are examined. The structure's chemical potential is examined along with its molecular orbital energies, E_{LUMO} and E_{HOMO}, three-dimensional (3D) surface image, molecular electrostatic potential (MEP), and dipole moment.We conducted the Hirshfeld surface analysis using CrystalExplorer version 3.1 to determine the intermolecular interactions between each atom.

2.6. *In Vitro and Ex Vivo* Biological Studies. The established method from scientific literature was followed for *in vitro* antioxidant, *ex vivo* anti-inflammatory, and *in vitro* α-GD, DPP-4, and MPO enzymatic inhibition studies.[56−60] Ascorbic acid and aceclofenac were used as positive controls for antioxidant and anti-inflammatory studies, respectively. For α-GD, DPP-4, and MPO enzymatic inhibition studies, acarbose, sitagliptin, and salicylhydroxamic acid were used as positive controls, respectively. The complete procedures for the biological studies are given in the SI.

https://doi.org/10.1021/acsomega.3c07555
ACS Omega 2024, 9, 7850−7868

Table 3. X-ray Details of MDC and ADC[a]

	MDC	ADC
chemical formula	$C_{16}H_{14}N_2O_6$	$C_{16}H_{12}N_2O_6$
formula weight	330.29 g/mol	328.28 g/mol
temperature	298(2) K	300(2) K
wavelength	0.71073 Å	0.71073 Å
crystal size	0.098 mm × 0.170 mm × 0.200 mm	0.120 mm × 0.145 mm × 0.186 mm
crystal system	monoclinic	monoclinic
space group	$P12_11$	$P12_1/c$ 1
unit cell dimensions	a = 4.9569(5) Å	a = 16.823(3) Å
	b = 8.3653(8) Å	b = 7.2581(12) Å
	c = 18.1827(18) Å	c = 11.904(2) Å
	α = 90°	α = 90°
	β = 95.723(3)°	β = 97.046(5)°
	γ = 90°	γ = 90°
volume	750.20(13) Å^3	1442.5(4) Å^3
Z	2	4
F(000)	344	680
density (calculated)	1.462 g/cm^3	1.511 g/cm^3
absorption coefficient	0.114 mm^{-1}	0.118 mm^{-1}
theta range for data collection	2.25−28.30°	2.44−28.29°
index ranges	$-6 \le h \le 6, -11 \le k \le 11, -24 \le l \le 24$	$-22 \le h \le 22, -9 \le k \le 9, -15 \le l \le 15$
reflections collected	21,073	32,344
independent reflections	3701 [R(int) = 0.0420]	3569 [R(int) = 0.0561]
refinement method	full-matrix least-squares on F^2	full-matrix least-squares on F^2
data/restraints/parameters	3701/1/221	3569/0/218
goodness-of-fit on F^2	1.076	1.067
final R indices [$I > 2\sigma(I)$]	R_1 = 0.0389	R_1 = 0.0483
	wR_2 = 0.0824	wR_2 = 0.1108
R indices [all data]	R_1 = 0.0623	R_1 = 0.1015
	wR_2 = 0.0963	wR_2 = 0.1463
largest diff. peak and hole	0.139 and −0.147 e Å^{-3}	0.230 and −0.171 e Å^{-3}

[a]Computer programs: Bruker APEX4/SAINT, SHELXL2019/1 (Sheldrick, 2019), and Bruker SHELXTL.

3. RESULTS AND DISCUSSION

3.1. Pharmacokinetic Studies. *3.1.1. Drug-Likeness.* The Lipinski's rule of five is used to assess a molecule's medicinal similarity. According to Lipinski, any oral medicine should have the following properties: a molecular weight (MW) of ≤500, a partition coefficient (log P) of ≤5, a number of rotatable bonds of ≤10, and a number of hydrogen-bond donors and acceptors of ≤5 and ≤10, respectively.[61−63] Molecules must meet all five criteria for use in medication delivery. Any molecule that satisfies Ghose's law must have the following properties: a molecular weight between 160 and 480, a log P value between −0.4 and 5.6, a molar refractive range between 40 and 130, and an overall atom count between 20 and 70.[64] Veber's rule states that a standard drug to have good oral bioavailability should meet the following criteria: rotatable bonds ≤10 and TPSA ≤ 140 Å^2.[65] According to Egan, good oral bioavailability standards are TPSA ≤ 130 Å^2 and log P values within the limit of $-1.0 \le \log P \le 5.8$.[66] To distinguish between compounds that are similar to drugs and those that are not, Muegge's rule modified the characteristics range and added more factors. According to Muegge's rule, the ideal MW and log P ranges are 200−600 and −2 to 5, respectively. Additionally, there should be more than four total carbon atoms, at least one heteroatom, and seven or fewer rings. According to Muegge, the hydrogen-bond acceptors and donors must be ≤5 and ≤10, respectively, and the rotatable bond must be ≤15.[67] Using the web resources SwissADME and ChemDraw Professional 16.0, the drug-likeness rules are anticipated. Table 4 shows that the MDC and ADC molecules adhere to all five rules without any deviation. Results from MW, HBA, and HBD suggest that the compounds have significant levels of penetration and absorption in the body. The total polar surface areas (TPSAs) of the MDC and ADC molecules are, respectively, 102.612 and 110.45 Å^2. TPSA is described as the overall surface sum of polar molecules or atoms (oxygen and nitrogen) and their hydrogen attachments. TPSA predicts cellular absorption, and the ideal range for absorption is 60−140 Å^2.[68] Table 5 shows that MDC and ADC each have a bioavailability score of 55%. Bioavailability is the rate at which a molecule enters the bloodstream and reaches the site of action. Any moiety with a bioavailability score of ≥0.55 is considered ideal and absorbed very well by the body.[69] A bioavailability score of 0.55 and a TPSA score between 60 and 140 Å^2 indicate optimal absorption for both MDC and ADC. Owing to their high bioavailability scores and flexibility, MDC and ADC can quickly enter the body's systemic circulation, go to the site of action, and engage the binding pocket of biomolecules.

Table 5. Drug-Likeness Prediction for the Proposed Molecules

compound	Lipinski	Ghose	Veber	Egan	Muegge	bioavailability score
MDC	yes	yes	yes	yes	yes	0.55
ADC	yes	yes	yes	yes	yes	0.55

3.1.2. In Silico ADMET Prediction. *In silico* ADMET prediction is a crucial drug profiling step in the process of discovering new medicines. Table 6 summarizes the *in silico* ADMET parameters for MDC and ADC ligands, using online free tools SwissADME, pkCSM, and ProTox-II. The ADMET predictions for the well-known methylenedioxyphenyl-based drugs, piribedil (PB), berberine (BB), stiripentol (SP), and cinoxacin (CX), are calculated for a comparative study. Any

Table 4. Lipinski's Rule of Five for the Proposed Molecules

	descriptors					
compound	MW (molecular weight in g/mol)	log P (partition coefficient)	RB (rotatable bond)	HBA (hydrogen-bond acceptor)	HBD (hydrogen-bond donor)	TPSA (topological polar surface area in Å^2)
MDC	330.29	1.56	6	6	1	102.61
ADC	328.28	1.22	5	6	1	110.45

https://doi.org/10.1021/acsomega.3c07555
ACS Omega 2024, 9, 7850−7868

Table 6. *In Silico* ADMET Parameters for Proposed Molecules[a]

absorption							
Com	Ws (log mol/L)	Caco2-P (log in 10^{-6} cm/s)	HIA (% A)	SP (log K_p)	P-gs	P-GI i	P-GII i
PB	−2.55	1.30	96.15	−2.81	no	no	no
BB	−3.20	1.62	100	−2.67	no	no	yes
SP	−3.09	1.89	92.85	−2.28	no	no	no
CX	−3.20	1.26	78.86	−2.73	no	no	no
MDC	−3.71	0.37	90.84	−2.74	yes	no	no
ADC	−3.60	0.33	96.29	−2.73	yes	no	no

distribution				
	HVDss (log L/kg)	Hf (Fu)	BBB permeability (log BB)	CNS permeability (log PS)
PB	0.24	0.35	−0.025	−2.515
BB	0.81	0.35	0.633	−1.675
SP	0.23	0.13	0.267	−1.677
CX	−0.66	0.33	−0.653	−3.043
MDC	−0.44	0	−0.603	−2.533
ADC	−0.49	0.05	−0.552	−2.365

metabolism							
PC-4	CYP2D6 Sub	CYP3A4 Sub	CYP1A2 In	CYP2C19 In	CYP2C9 In	CYP2D6 In	CYP3A4 In
PB	no	yes	yes	no	no	no	no
BB	no	yes	yes	no	no	yes	no
SP	no	yes	yes	yes	no	no	no
CX	no	no	no	no	no	no	no
MDC	no	yes	yes	yes	yes	no	yes
ADC	no	yes	no	yes	yes	no	yes

excretion		
	total clearance (log mL/min/kg)	renal OCT2 Sub
PB	0.855	yes
BB	1.272	yes
SP	−0.008	no
CX	0.643	no
MDC	0.171	no
ADC	0.039	no

toxicity										
	AMES	HTD (log mg/kg/day)	h I inh	h II inh	OAT (LD_{50}) mol/kg	OCT (LOAEL) (log mg/kg/D)	HT	SS	TP-T (log μg/L)	MT (log mM)
PB	no	−0.54	no	yes	2.929	1.384	yes	no	0.386	0.032
BB	no	−0.132	no	no	3.313	1.275	no	no	0.288	−0.869
SP	no	0.219	no	no	1.959	2.156	no	yes	2.211	0.811
CX	yes	0.87	no	no	1.956	1.004	yes	no	0.284	2.66
MDC	yes	0.154	no	no	2.122	1.548	yes	no	0.34	−0.061
ADC	yes	0.18	no	no	2.117	1.476	yes	no	0.327	0.603

[a]PC, positive control; Com, compound; Ws, water solubility; Caco2-P, Caco2-permeability; HIA, human intestinal absorption; SP, skin permeability; P gs, P-glycoprotein substrate; P gIi, P-glycoprotein I inhibitor; P-gIIi, P-glycoprotein II inhibitor; HVDss, steady-state volume of distribution; Hf, fraction unbound (human); BBB, blood−brain barrier; CNS, central nervous system; CYP, cytochrome *P*; Sub, substrate; In, inhibitor; OCT2, organic cation transport 2; HTD, maximum tolerated dose (human); OAT, oral rat acute toxicity (LD_{50}); OCT, oral rat chronic toxicity (LOAEL); HT, hepatotoxicity; SS, skin sensitization; TP-T, *Tetrahymena pyriformis* toxicity; MT, Minnow toxicity.

drug molecule administered to the body needs to be first absorbed by the body and then be able to be removed from the body with the fewest negative effects possible. Every molecule must be water soluble to be a medicine molecule because the human body is composed of about 60% water. The Cancer coli-2 (Caco-2) cell line, which is made up of human epithelial colorectal adenocarcinoma cells, effectively absorbs anything with a Caco-2 permeability score of more than 0.90. The majority of medications taken by mouth must be absorbed in the intestines, and any molecule that absorbs more than 30% is regarded as having exceptional absorption. MDC and ADC have HIA values greater than 90%, indicating adequate intestine absorption. The boiled egg diagram between TPSA and partition coefficient (log *P*) can predict the molecule's ability to traverse the blood−brain barrier (BBB) or human intestinal absorption (HIA).[70] The egg yolk represents the BBB, whereas the white albumin of the egg stands in for HIA.[71] Figure 2 depicts the penetration of PB, SP, and BB through BBB whereas CX, MDC, and ADC through HIA. The log K_p value greater than 2.5 denotes low skin permeability for PB, BB, CX, MDC, and ADC. The bioavailability radar plot is depicted in Figure 3 for the drugs PB, BB, SP, CX, MDC, and ADC. The steady-state volume of distribution (VDss) refers to the amount of medication needed for an even distribution to produce a blood plasma-like concentration. The higher VDss value denotes that the tissue has a more extensive drug

https://doi.org/10.1021/acsomega.3c07555
ACS Omega 2024, 9, 7850−7868

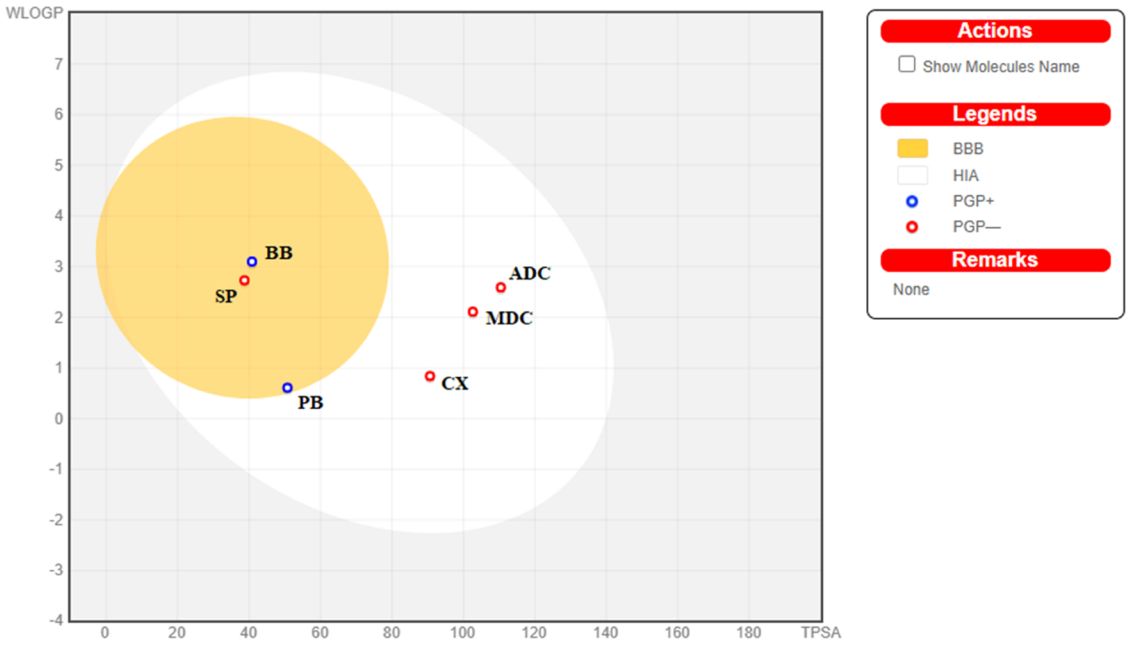

Figure 2. Boiled egg diagram for piribedil (PB), berberine (BB), stiripentol (SP), cinoxacin (CX), MDC, and ADC.

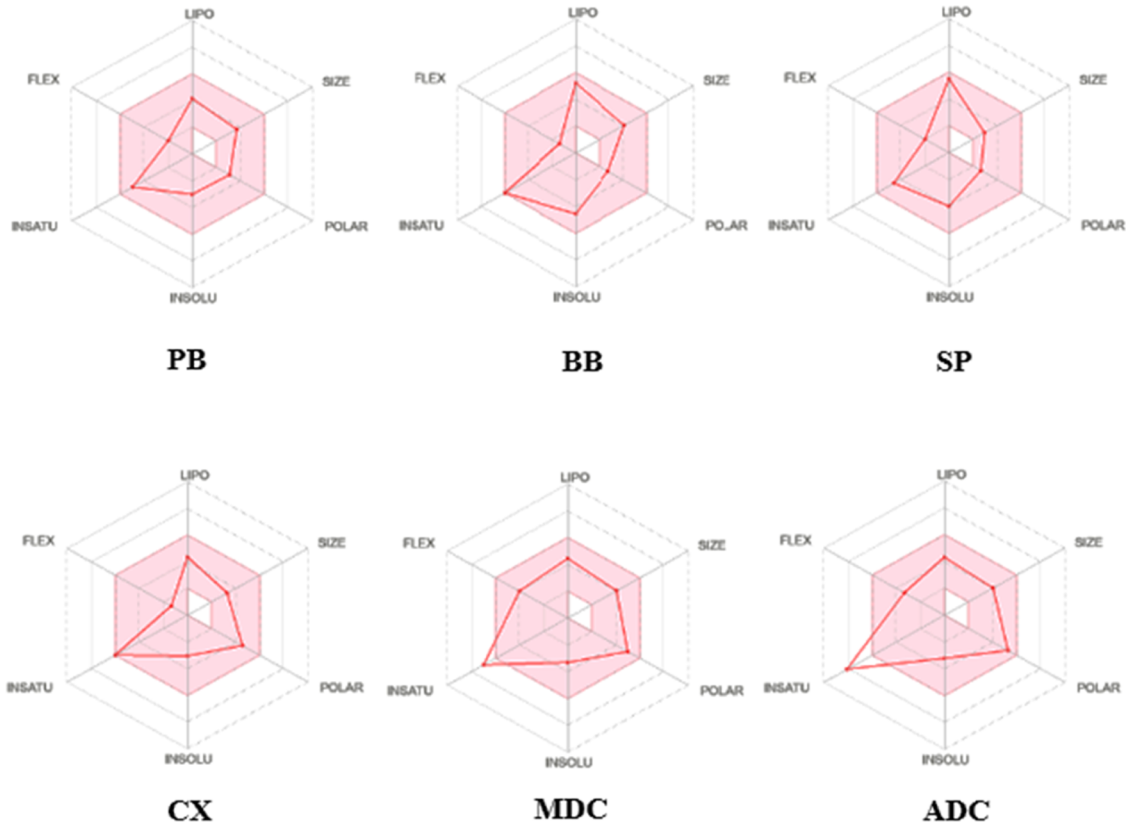

Figure 3. Bioavailability radar for piribedil (PB), berberine (BB), stiripentol (SP), cinoxacin (CX), MDC, and ADC.

dispersion than plasma. Log VDss value is optimum within the range $-0.15 \geq$ log VDss ≥ 0.45. The VDss values for MDC and ADC are both more than -0.15, indicating a good volume of dispersion. Having log PS values of -2.5 and -2.3, respectively, which are greater than -2, MDC and ADC are able to quickly enter the central nervous system (CNS). The Cytochrome P450 (CYP) family of enzymes, which metabolizes 50% of medications by itself, is essential for the metabolism of substances. The liver's detoxifying enzyme Cytochrome P450 oxidizes xenobiotics to encourage excretion. The drug molecule must be processed by one of two CYP450 isoforms, CYP2D6 or CYP3A4, which are linked to drug metabolism. Except for CX, all substances can be metabolized by CYP3A4 substrates. The sum of renal clearance and hepatic clearance determines the total clearance, which is correlated with bioavailability. All of the compounds have extremely low

https://doi.org/10.1021/acsomega.3c07555
ACS Omega 2024, 9, 7850−7868

Table 7. Binding Energy and Interaction of Proteins with Positive Controls, MDC, and ADC

protein	ligand	binding energy (kcal/mol)	binding interaction
α-GD	acarbose	−4.61	ASP:69, TYR:72, HIS:112, TYR:158, ASP:215, VAL:216, LEU:219, ARG:315, ARG:446
	MDC	−3.83	TYR:158, ASP:215, ASP:216, GLN:279, HIS:280, SER:311, PRO:312, PHE:314, ARG:315, ASP:352
	ADC	−2.67	LYS:156, TYR:158, LEU:313, ARG:315, GLU:411, ASN:415
DPP-4	sitagliptin	−5.66	GLU:205, GLU:206, PHE:357, TYR:547, TRP:629, SER:630, HIS:740
	MDC	−5.30	ARG:125, HIS:126, GLU:206, SER:209, SER:630, TYR:631, VAL:656, TRP:659, TYR:666
	ADC	−4.20	TYR:553, GLN:553, LYS:554, TRP:629
MPO	salicylhydroxamic acid	−7.88	GLY:90, TYR:296, MET:87, PHE:332
	MDC	−7.79	GLU:242, ARG:333, LEU:406, LEU:417, LEU:420, ARG:424
	ADC	−7.74	GLU:102, ARG:333, LEU:217, LEU:420, ARG:424

clearance indices, which indicates greater drug persistence in the body. Lethal dose 50 (LD_{50}), AMES toxicity (*Salmonella typhimurium* reverse mutation assay), and hepatotoxicity are the three basic toxicological parameters used to interpret the toxicity of the compounds. AMES can determine which molecules are more hazardous and which molecules are mutagenic based on their LD_{50} values. In general, a drug's maximum tolerated dose (HTD) should not be more than 0.47. The estimated hazardous dosage of chemicals in humans is minimal because the HTD values for MDC and ADC are 0.15 and 0.18, respectively, which are both less than 0.47. According to the toxicity prediction, the compounds are either nontoxic or only tolerably poisonous to a certain degree.[72−74] The proposed MDC and ADC compounds exhibit drug similarity based on *in silico* predictions and are suitable for the drug development process.

3.2. Molecular Docking. A docking investigation is conducted to determine the binding interaction between MDC and ADC and the residues in the active sites of MPO, DPP-4, and α-GD.[75] Table 7 provides examples of the ligand−protein interactions and binding energies of MDC and ADC to the proteins. Salicylhydroxamic acid, sitagliptin, and acarbose, recognized for inhibiting MPO, DPP-4, and α-GD, are used as positive controls. Figure 4 shows images of positive controls, MDC, and ADC docked with proteins in two dimensions. The binding energy value assesses both the stability of the protein−ligand complex and the intensity of the interaction between a protein and a ligand. Lower binding energy encourages a stronger association between the protein and the ligand and helps the targeted protein form stable complexes that are well suited for biological function.

Compared with the positive control (−5.88 kcal/mol), MDC and ADC appear to have higher binding energies, according to docking scores of MPO (−7.79 and −7.74 kcal/mol, respectively). The oxygen in the nitro group and ARG:333 and ARG:424 form a hydrogen bond in both molecules. To maintain the stability and specificity of the protein−ligand complex, many intermolecular hydrogen bonds are extremely important. MDC and ADC achieved docking scores of −4.30 and −4.20 kcal/mol for DPP-4, respectively. Positive controls have a higher binding score (−7.66 kcal/mol) than do MDC and ADC.

MDC interacts with amino acids ARG:125, HIS:126, SER:209, SER:630, and TYR:631 via intermolecular hydrogen bonding. Three groups in the ligand, the methylenedioxy, nitro, and methoxy groups, are primarily where hydrogen bonds are formed. Through hydrogen bonds, amino acids GLN:553 and LYS:554 bind to the protein in ADC. MDC and ADC achieved docking scores of −3.83 and −4.67 kcal/mol with α-GD, respectively. GLN:279, HIS:280, and ARG:315 for MDC and LYS:156 and ASN:415 for ADC are the hydrogen-bond interactions. Methylenedioxy bridge and nitro group both produce hydrogen bonds. When docked with MPO, DPP-4, and α-GD, the MDC and ADC molecules fit well into active site pockets and exhibit positive interactions with proteins.

In conclusion, MDC exhibits more hydrogen bonds and binding energy than ADC, and it exhibits potential ligand−protein interactions with excellent docking stability. In brief, we may deduce from the docking studies that the MDC ligand exhibits the best binding and that, in comparison with other proteins, it binds to MPO specifically.

3.3. Structure−Activity Relationship (SAR). Based on the *in silico* results and structure−activity relationship, we plan to synthesize MDC and ADC and proceed with further screening. Both MDC and ADC have key functional groups, nitro, diether, and amide, in common (Figure 5). Nitro substitution in the parent aromatic ring has a positive electrostatic potential which can interact with the proteins - carbonyls, sulfurs, and water via "π−hole interaction".[76] Molecular electrostatic potential studies conducted for MDC and ADC substantiate this result. The presence of amide bonds is another salient feature for a better bioactivity. The carbonyl group and the amine group, which may function as a hydrogen-bond acceptor (HBA) and a hydrogen-bond donor (HBD), respectively, are two different types of hydrogen-bonding sites that are often present in an amide.[77] This feature helps amides form hydrogen-bonding interactions with biomolecules. The presence of the methylenedioxyphenyl pharmacophore in the molecules further enhances the bioactivity. Nucleophilic oxygen in the diether functional group readily donates electrons to interact with protein residues for facilitating biological interactions. Upon comparing MDC and ADC, MDC has an electron-donating methoxy group that readily donates electrons with biomolecules. The role of the methoxy group in many phytochemicals like curcumin[20] and resveratrol is significantly explored and proven in many scientific studies.[78,79] The acetophenone group is an electron-withdrawing group, and it can accept electrons from biomolecules to form an electrovalent bond. The conducted *in vitro* study results also suggest that MDC has better inhibition capacity than ADC. This might be due to the presence of electron-donating methoxy substitution which readily interacts with the residues in the active site pocket of the protein.

3.4. Characterization. *3.4.1. NMR and IR.* 6-Nitrobenzo-[1,3]dioxole-5-carboxylic acid: The purified product was analyzed for ^{1}H and ^{13}C NMR using dimethyl sulfoxide (DMSO) as solvent in 0 delta TMS calibration method. In

https://doi.org/10.1021/acsomega.3c07555
ACS Omega 2024, 9, 7850−7868

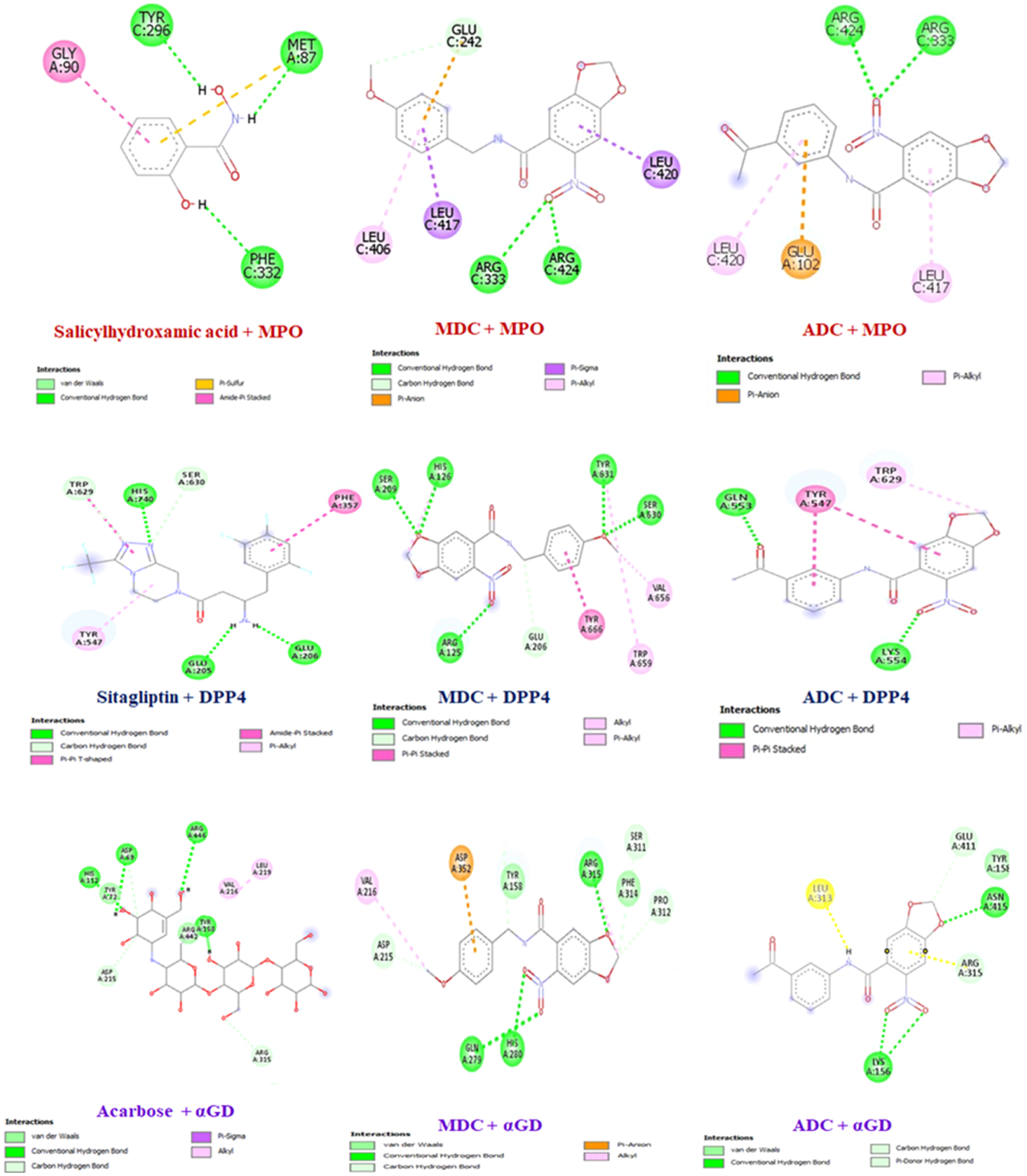

Figure 4. Two-dimensional (2D) molecular docking binding interaction images of salicylhydroxamic acid, sitagliptin, acarbose, MDC, and ADC with myeloperoxidase (MPO), dipeptidyl peptidase-4 (DPP-4), and α-glucosidase (α-GD) proteins.

proton NMR, $-CH_2-$ in the methylenedioxy bridge appeared as a singlet at 6.21 ppm, and in carbon NMR, the characteristic acid carbonyl peak appeared at 166.1 ppm. Detailed analysis data are available in the SI.

N-(4-Methoxybenzyl)-6-nitrobenzo[1,3]dioxole-5-carboxamide (MDC): In proton NMR, the characteristic amide $-NH-$ was observed as a triplet at 9.00 ppm, and the $-CH_2-$ proton of the methylenedioxy bridge and the methoxy proton appeared as singlets at 6.27 and 3.74 ppm, respectively. In carbon NMR, the characteristic amide carbonyl and methoxy carbon appeared at 165.5 and 55.5 ppm, respectively. The functional groups in MDC are confirmed using FT-IR analysis. The characteristic amide stretch (N−H) is observed at 3278.99 cm^{-1}, the carbonyl group (−C═O−) stretch at

https://doi.org/10.1021/acsomega.3c07555
ACS Omega 2024, 9, 7850−7868

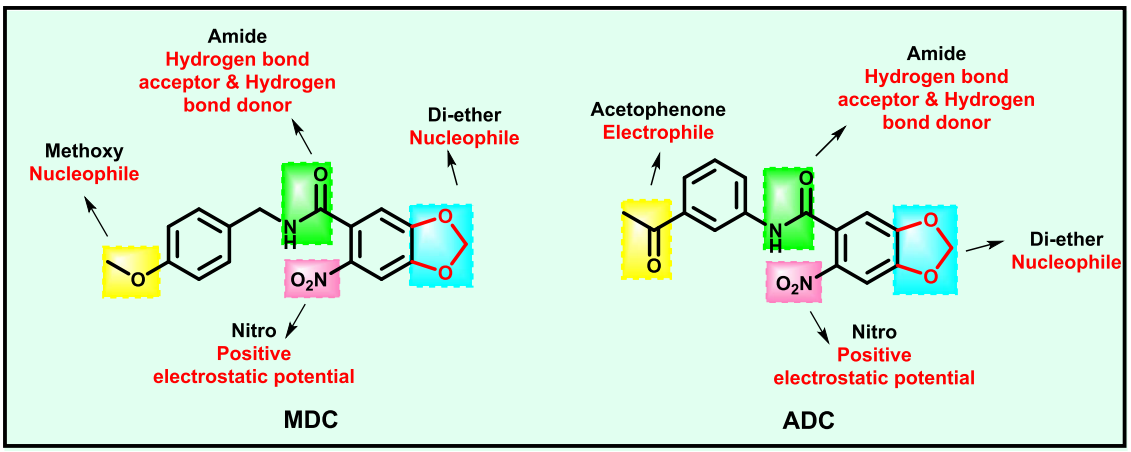

Figure 5. Structure−activity relationship of MDC and ADC.

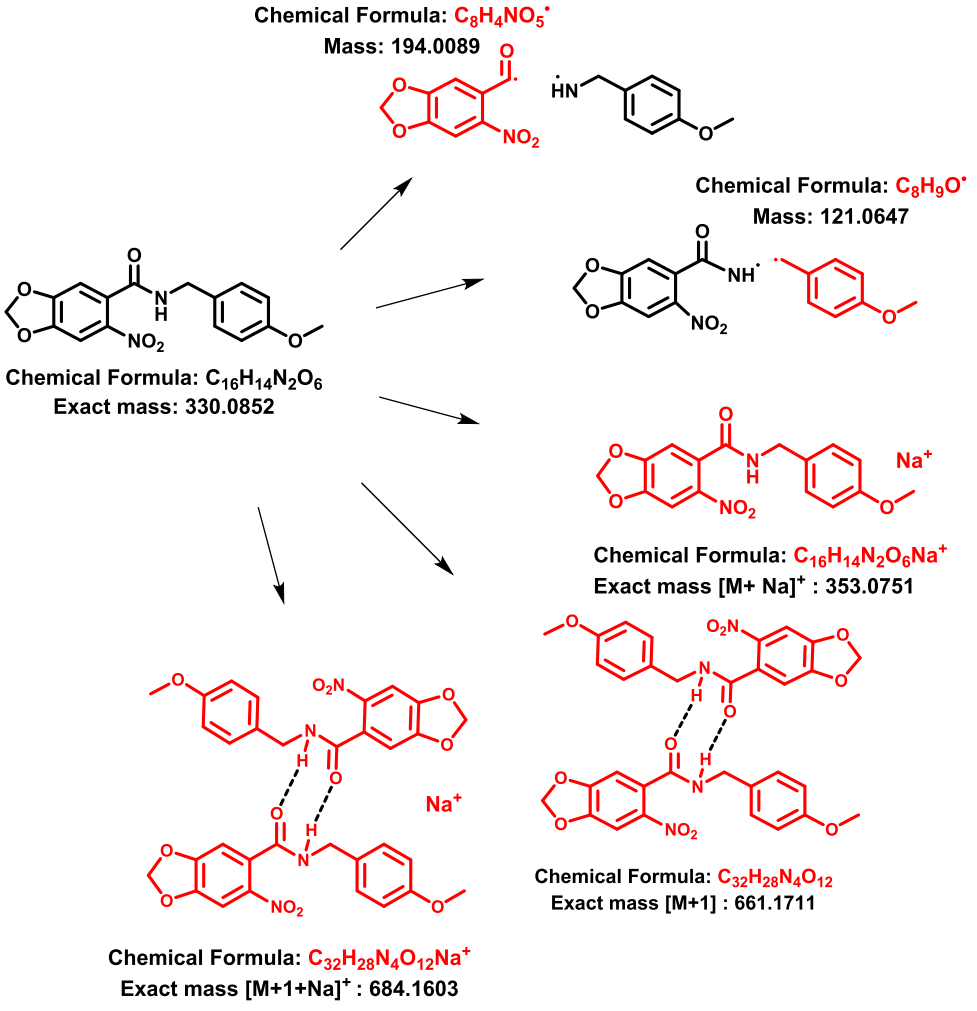

Figure 6. Mass fragmentation pattern of MDC.

1643.16 cm^{-1}, and the NO_2 stretch at 1501 cm^{-1} (asymmetrical) and 1345.97 cm^{-1} (symmetrical).

N-(3-Acetylphenyl)-6-nitrobenzo[1,3]dioxole-5-carboxamide (ADC): In proton NMR, the amide −NH− is identified as a singlet at 10.73 ppm. The $-CH_2-$ proton of the methylenedioxy bridge and the methyl proton of acetophenone appeared as singlets at 6.32 and 2.58 ppm, respectively. In carbon NMR, acetophenone carbonyl and amide carbonyl are observed at 198.0 and 164.4 ppm, respectively. Acetophenone methyl carbon appeared at 27.2 ppm. FT-IR analysis validates the functional groups in ADC. The characteristic amide stretching (N−H) is detected at 3311.45 cm^{-1}, the carbonyl group stretching (−C═O−) at 1666.50 cm^{-1}, and the NO_2 stretching at 1602.8 cm^{-1} (asymmetric) and 1338.60 cm^{-1} (symmetric).

https://doi.org/10.1021/acsomega.3c07555
ACS Omega 2024, 9, 7850−7868

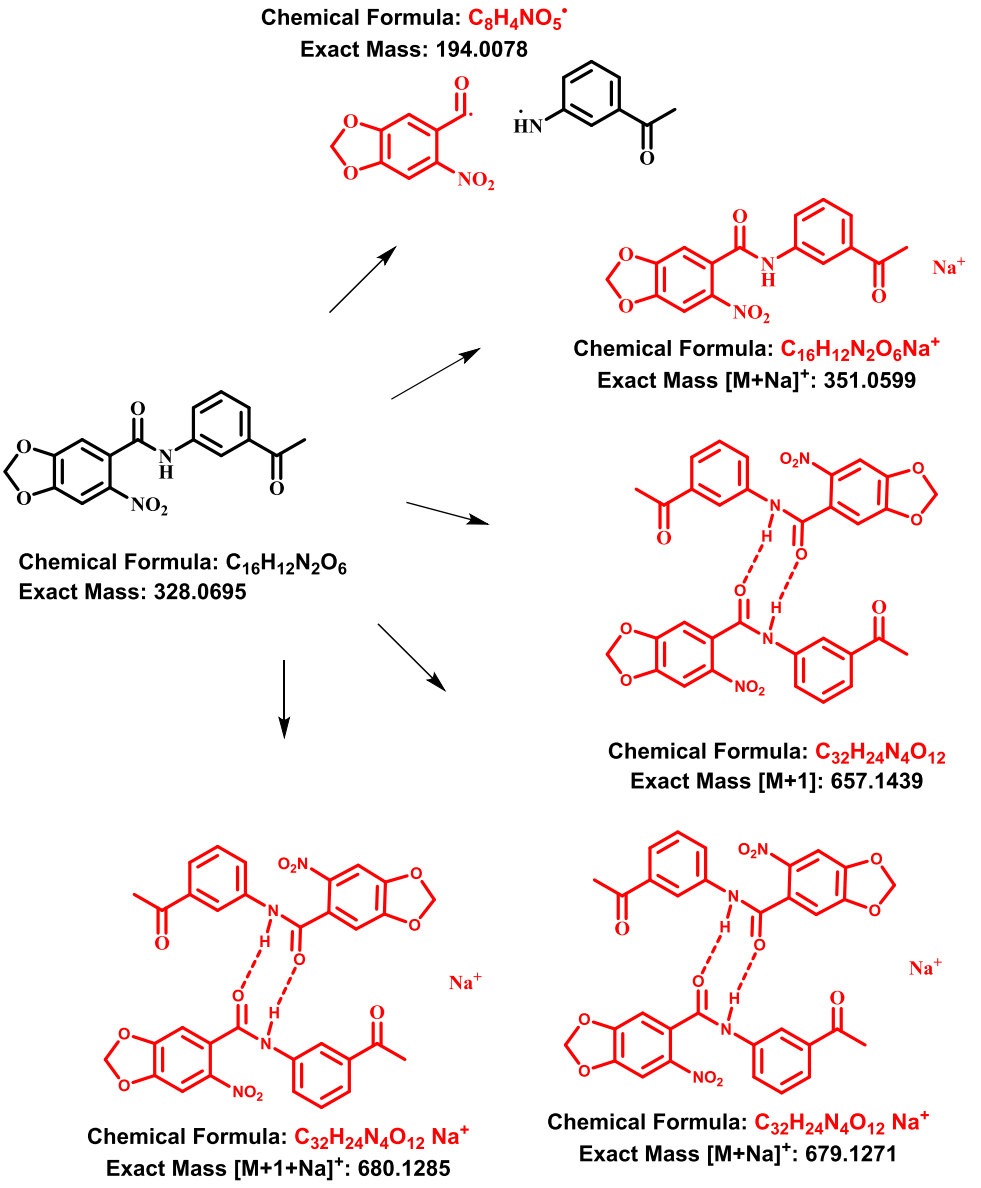

Figure 7. Mass fragmentation pattern of ADC.

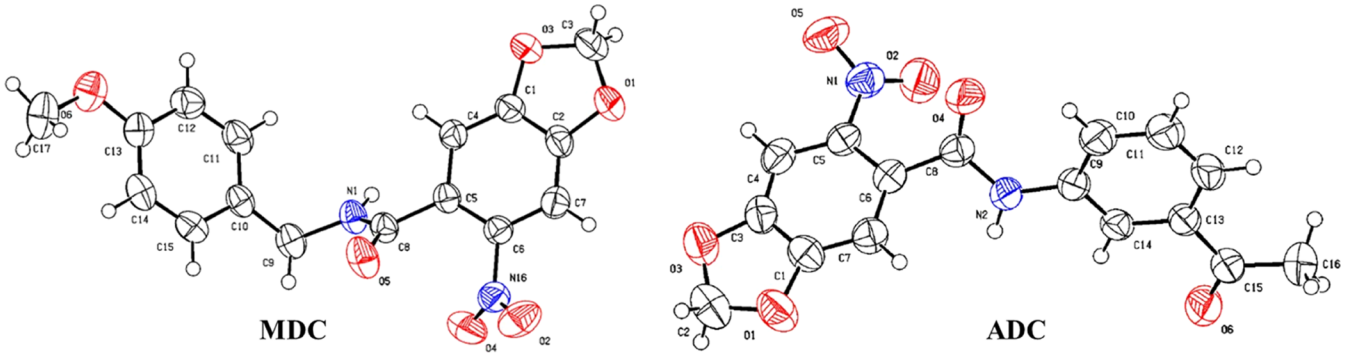

Figure 8. ORTEP diagram for the crystal structure.

3.4.2. Mass Spectral Data. The exact mass of *N*-(4-methoxybenzyl)-6-nitrobenzo-[1,3]-dioxole-5-carboxamide (MDC) is 330.0852, and 331.0932 is the measured mass in positive mode [M + 1]. We examined the pattern of mass spectral fragmentation to further support the predicted structure. The potential predicted MDC fragments are $C_8H_4NO_5^{\bullet}$ and $C_8H_9O^{\bullet}$, with masses 194.0085 and 121.0653, respectively. A possible dimer is $C_{32}H_{28}N_4O_{12}$, which has a calculated mass of 661.1704. According to experimental data (Figure 6), the masses of the dimer

https://doi.org/10.1021/acsomega.3c07555
ACS Omega 2024, 9, 7850−7868

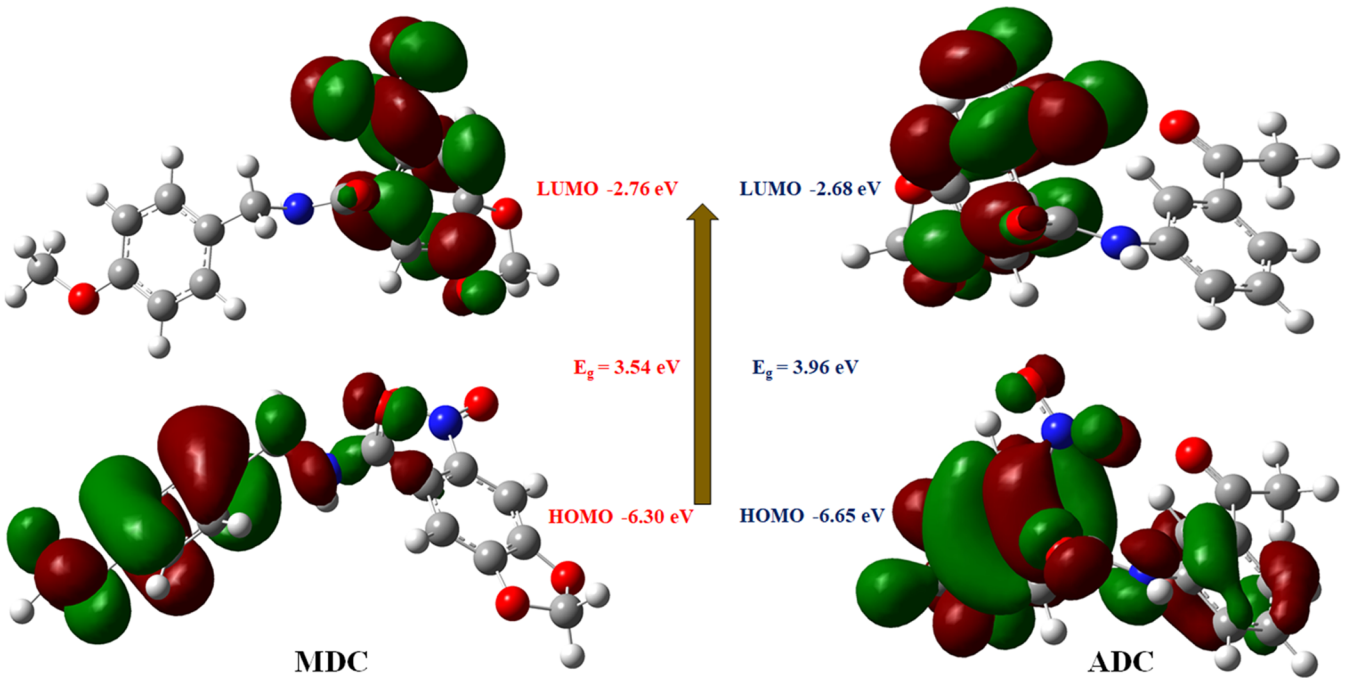

Figure 9. HOMO and LUMO electron distribution level.

$C_{32}H_{28}N_4O_{12}$ and the fragments $C_8H_4NO_5^{\bullet}$ and $C_8H_9O^{\bullet}$ are 661.1777 and 194.0085 and 121.0647, respectively. The theoretical masses of the fragments and the dimer agree well with the experimental data. Apart from these fragments, there are possibilities of sodium adduct formation,[80] which is shown in Figure 6.

The exact mass of *N*-(3-acetylphenyl)-6-nitrobenzo[1,3]-dioxole-5-carboxamide referred to as ADC is 328.0695, and 329.0766 is the mass obtained in positive mode [M + 1]. Here, only one fragment is observed; the expected mass for that fragment ($C_8H_4NO_5^{\bullet}$) is 194.0089, and the experimental mass is 194.0078. The theoretical mass agrees well with the experimental data. As in MDC above, we can see the formation of three sodium adducts, as shown in Figure 7. The original mass spectral file images of MDC and ADC are available in the SI.

3.5. Single-Crystal X-ray Diffraction Studies. Unquestionably, the crystallization process aids in determining the final architectures of MDC and ADC. The final crystals are seen in a 1:1 mixture of dimethyl sulfoxide and hexane after experiments with various techniques and solvent systems. At room temperature, a method of gradual solvent evaporation was used. SC-XRD analysis is performed on the produced crystals and the resultant ORTEP plot is shown in Figure 8. Bond angles and bond lengths from DFT (theoretical) and SC-XRD (calculated) are shown in S3.1.

For MDC, XRD data reveal that the methylenedioxyphenyl bridge, O3−C3, and O1−C3 show bond lengths of 1.43 and 1.42 Å, respectively with a bond angle of 105.4° for the O3−C3−O1 bond. The linking amide bond length of nitrogen and the adjacent methyl group (N1−C9) is 1.46 Å and that of nitrogen with the carbonyl group (N1−C8) is 1.32 Å. The corresponding bond angle for C8−N1−C9 is 121.7° and that for N1−C8−C5 is 115.9°. The amide carbonyl (C8−O5) bond length is 1.23 Å, and the bond angle for N1−C8−O5 is 123°. The bond length is 1.41 Å for O6−C17 in the methoxy carbon with a bond angle of 117.6° for C13−O6−C17. For the nitro group, the bond length of O2−N16 was slightly higher than that of O4−N6 with a bond angle of 124.4 for the O5−N1−O2 bond. With cell dimensions a = 4.9569(5) Å, b = 8.3653(8) Å, and c = 18.1827(18) Å, a single crystal is monoclinic with space group $P12_11$ and Z = 2.

For ADC, XRD data reveal that the methylenedioxyphenyl bridge, O3−C2, and O1−C2 show a bond length of 1.43 and 1.44 Å, respectively, with a bond angle of 108.29° for the O3−C2−O1 bond. The linking amide bond length of nitrogen and the benzene ring (N2−C9) is 1.40 Å and that of nitrogen with the carbonyl group (N2−C8) is 1.35 Å. The corresponding bond angle for C8−N2−C9 is 127.36° and that for N2−C8−C6 is 114.20°. The amide carbonyl (C8−O4) bond length is 1.20 Å, and the bond angle for N2−C8−O4 is 124.03°. The acetophenone carbonyl (C15−O6) bond length and bond angle (C16−C15−O6) are 1.22 Å and 120.4°, respectively. For the nitro group, the bond length of O5−N1 showed slightly higher bond length than O2−N1. The bond angle for the O5−N1−O2 bond was found to be 118.3°. When compared to amide carbonyl, acetophenone carbonyl has slightly greater values for bond length and bond angle. With cell dimensions a = 16.823(3) Å, b = 7.2581(12) Å, and c = 11.904(2) Å, a single crystal is monoclinic with space group $P12_1/c1$ and Z = 4.

These bond angles and lengths are in good agreement with theoretical calculations performed by DFT (Table S1). Comparable bond lengths exist between the methylenedioxy bridges of MDC and ADC, but ADC has a larger bond angle; similar to how the bond length of the amide group is longer in MDC and the bond angle is greater in ADC. The larger bond angle in ADC reveals that the atoms are more open and widely spaced away than those in MDC. Greater flexibility and rotation are made possible by larger bond angles. The atoms are tightly spaced, and the molecule is smaller in MDC. The link between two atoms weakens, becomes less stable, and is more susceptible to cleavage as the bond length increases.

https://doi.org/10.1021/acsomega.3c07555
ACS Omega 2024, 9, 7850−7868

3.6. Computational Studies. *3.6.1. Frontier Molecular Orbital Analysis (FMO).* To determine a molecule's chemical reactivity, the molecular orbital theory is frequently used. Gaussian-16 software is used to conduct quantum chemistry research at the B3LYP/6-311G** level of theory. The frontier electron theory's crucial component focuses on the highest occupied molecular orbital (HOMO) and lowest unoccupied molecular orbital (LUMO) energy orbitals. The HOMO and LUMO surfaces for MDC and ADC are shown in Figure 9. The electron-rich nature of HOMO tends to donate electrons, and the electron-deficient nature of LUMO accepts electrons. The nucleophilic heteroatoms like nitrogen in MDC and ADC readily donate electrons, facilitating bond formation. In MDC, the HOMO surface is located near the amide group and the methoxy-substituted aromatic ring. The nucleophilic-methoxy group in MDC can help in bond formation with biomolecules via electron sharing. Hydrogen-bonding sites of the amide group facilitate hydrogen-bond formation with the active site pocket of protein. In ADC, HOMO surfaces are occupied in the methylenedioxyphenyl ring, amide, and nitro group. The nucleophilic nature of the diether and the presence of heteroatoms like nitrogen and oxygen help in bond formation. For both MDC and ADC, the LUMO surface is located at the methylenedioxyphenyl ring. Deficiency of electrons is seen across the region, and it facilitates bond formation with electron-donating pockets of biomolecules by readily accepting electrons. The heteroatoms in the ADC−MDC that contribute to a negative charge are shown in red. Similarly, the atoms like carbon and hydrogen that contribute to a positive charge are indicated by green-colored surfaces.[81] The HOMO and LUMO energies for MDC and ADC are −6.30 and −2.76 eV and −6.65 and −2.68 eV, with energy gaps (ΔE) of 3.54 and 3.96 eV, respectively. Higher energy gap molecules are typically more stable and less polarizable, resulting in the hardness of the entity. On the other hand, due to the molecules' strong polarizability, and narrow energy gap, molecules tend to exhibit chemical softness.[82] Pearson described chemical hardness as the energy gap between two FMOs.[83] The energy gap for ADC is higher when compared to MDC, suggesting that ADC shows chemical hardness and is more stable. The presence of an electron-withdrawing carbonyl group in acetophenone substitution increased the hardness of ADC when compared to MDC.

Global chemical reactivity parameters—global hardness, global softness, chemical potential, electron negativity, and global electrophilicity index—are calculated using Koopman's theorem.[84,85] Table 8 depicts the global chemical reactivity parameters. Electronegativity is a term used to describe an atom's or functional groups' ability to pull inbound electrons to itself.[86] The electronegative groups nitro and carbonyl in MDC and ADC have a tendency to accept the electrons facilitating bond formation with biomolecules. The global electrophilicity index represents the stabilization energy of the molecule. A smaller global electrophilicity index implies a strong nucleophilic molecule, while a higher value denotes a strong electrophilic molecule. Molecules are classified as potent electrophiles if values are greater than 1.5 eV, moderate electrophiles if values range in between 0.8 and 1.5 eV, and minor electrophiles if the values are less than 0.8 eV.[87,88] The electrophilicity index value for MDC and ADC is larger than 1.5 eV, indicating that the molecules have a potent electrophilic nature that facilitates the formation of bonds with biomolecules. Molecules having greater HOMO−LUMO energy gap show lesser tendency for interaction and bond formation, while molecules with less HOMO−LUMO energy gap are more interactive and are more willing to participate in chemical events involving bond breaking or bond formation. As can be seen from the DFT values, MDC has low HOMO−LUMO values, and it is anticipated to participate in the bond formations like covalent, hydrogen, and ionic bonds.

Table 8. DFT Molecular Orbital Energy Calculations

	energy	
DFT analysis	MDC	ADC
dipole moment	6.24 D	8.46 D
E (HOMO)	−6.30 eV	−6.65 eV
E (LUMO)	−2.76 eV	−2.68 eV
ΔE (HOMO−LUMO)	3.54 eV	3.96 eV
electronegativity (χ)	4.53	4.67
chemical potential (μ)	−4.53	−4.67
global hardness (η)	1.7	1.9
softness (σ)	0.28	0.50
global electrophilicity index (ω)	5.79	5.50

3.6.2. Hirshfeld Surface Calculations. To get a qualitative understanding of the role of the principal intermolecular interaction within the crystal, Hirshfeld surface (HFS) analysis, a graphical visualization technique, was performed.[89] Based on the crystallographic information file (CIF), the computational tool CrystalExplorer 3.1 is used to assess the molecular Hirshfeld surface analysis and its accompanying two-dimensional fingerprint plots. With the use of the fundamental energy model B3LYP/6-31G(d,p), the HFS analysis is used to determine the overall interaction energy of the crystal structure. With the help of d_{norm}, it is possible to identify molecular sites crucial for intermolecular interaction. Equation 1 is utilized to pinpoint the crystal compounds' surface areas that are especially important for intermolecular interactions. The normalized contact distance d_{norm} can be correlated with the radii of the atoms (vdW),[90,91] the distance to the closest nucleus interior to the surface (d_i), and the distance to the closest nucleus exterior to the surface (d_e).

$$d_{norm} = \frac{(d_i - r_i^{vdW})}{(r_i^{vdW})} + \frac{(d^e - r_e^{vdW})}{r_e} \quad (1)$$

Spackman and Jayatilaka's[89] approach offers insightful information regarding the strength of intermolecular interactions inside crystal structures. Intermolecular hydrogen bonds are crucial for the interaction of drugs with macromolecules. Figures 10 and 11 show the Hirshfeld surface with d_{norm} visualization graphs of MDC and ADC and two-dimensional (2D) fingerprint plots of intermolecular interaction surfaces, respectively. The nearest contacts are shown in red in d_{norm}, the farthest contacts in blue, and the contacts equivalent to the sum of the van der Waals radii[92] are shown in white regions. On Hirshfeld surfaces that are mapped using the shape index, red and blue triangular pairings may be seen interacting. This is additional proof that stacking interactions occur. Table 9 provides information about the molecule's surface characteristics.

From the Hirshfeld surface analysis, the corresponding volume (368.22 Å^3), asphericity (0.274), inner area (344.05 Å^2), and globularity (0.722) of MDC are calculated. According to the 2D fingerprint diagram, the d_i vs d_e of the crystal and

https://doi.org/10.1021/acsomega.3c07555
ACS Omega 2024, 9, 7850−7868

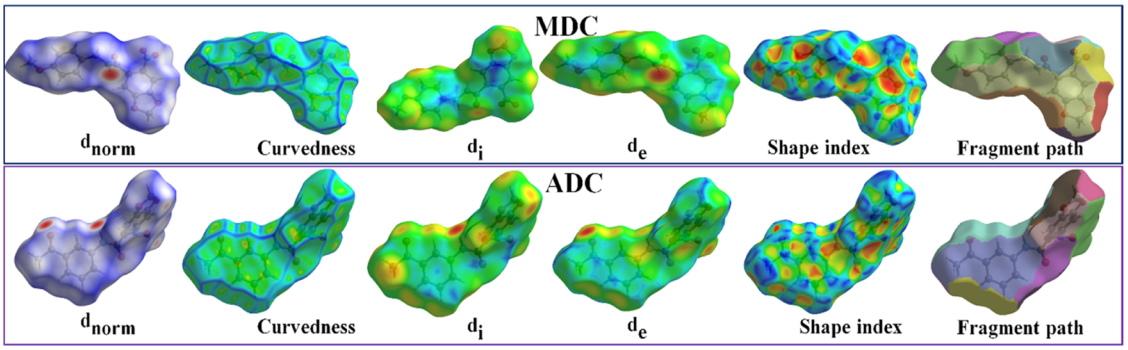

Figure 10. Hirshfeld surface maps for MDC and ADC.

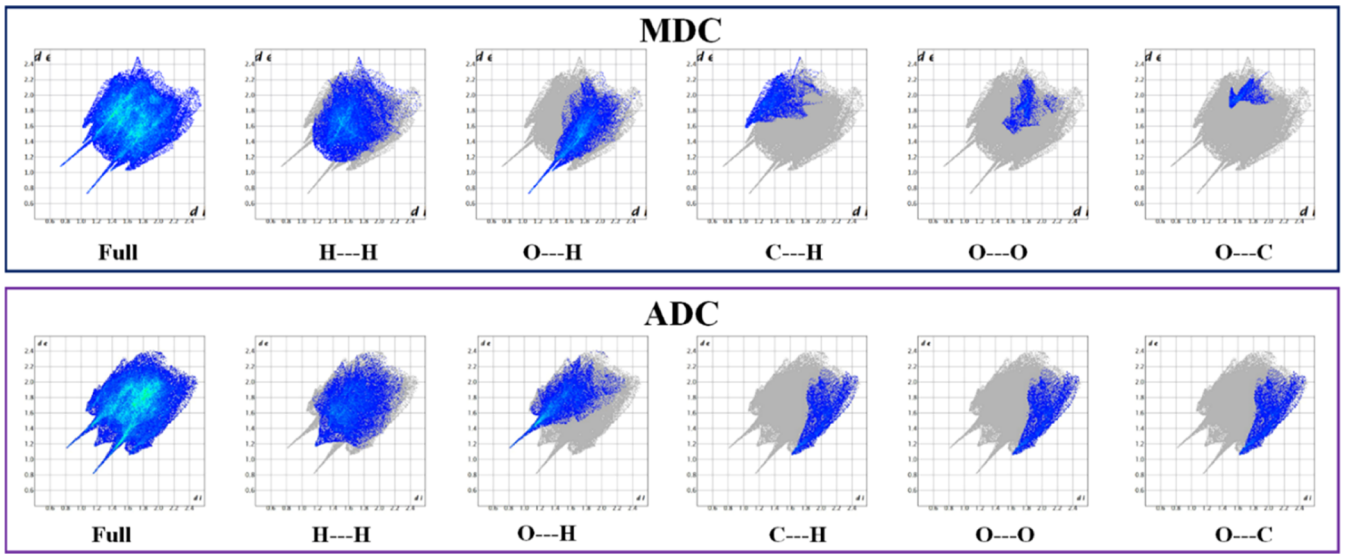

Figure 11. Full and disaggregated 2D fingerprint plot for the specific contacts.

Table 9. Surface Property Information

	MDC		ADC	
name	minimum	maximum	minimum	maximum
d_i	0.743	2.569	0.818	2.527
d_e	0.743	2.522	0.818	2.409
d_{norm}	−0.601	1.194	−0.487	1.665
shape index	−0.999	0.999	−0.992	0.998
curvedness	−3.853	0.259	−3.851	0.356

important contacts for crystal packing are found to be H···H (31.1%), O···H (20.5%), C···H (10.6%), O···O (3.4%), O···C (2.9%), C−C(1.1%), O···N (0.5%), H···N (0.5%), and N···C (0.1%). Similarly, for ADC, the corresponding volume, asphericity, inner area, and globularity are found to be 353.85 Å^3, 0.313, 334.08 Å^2, and 0.724, respectively. From the 2D fingerprint diagram, important contacts for crystal packing are H···H (26.5%), O···H (20.4%), C···H (8.0%), O···O (4.9%), O···C (4.1%), C···C(5.4%), O···N (0.6%), H···N (0.9%), and N···C (0.0%).

In 2D fingerprint diagrams, more than 25% of interactions in both MDC and ADC are for the H···H interaction. Both ADC and MDC have 20% of O···H interactions. The O···H bonding interactions are shown by the bright red point in the d_{norm}

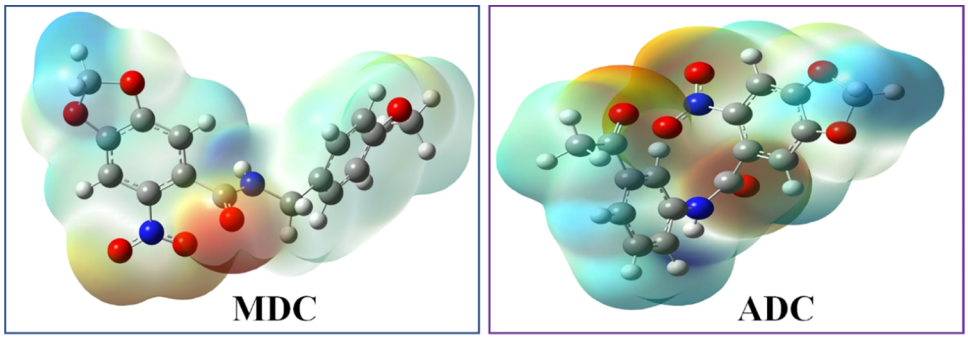

Figure 12. Molecular electrostatic potential surfaces for MDC and ADC.

https://doi.org/10.1021/acsomega.3c07555
ACS Omega 2024, 9, 7850−7868

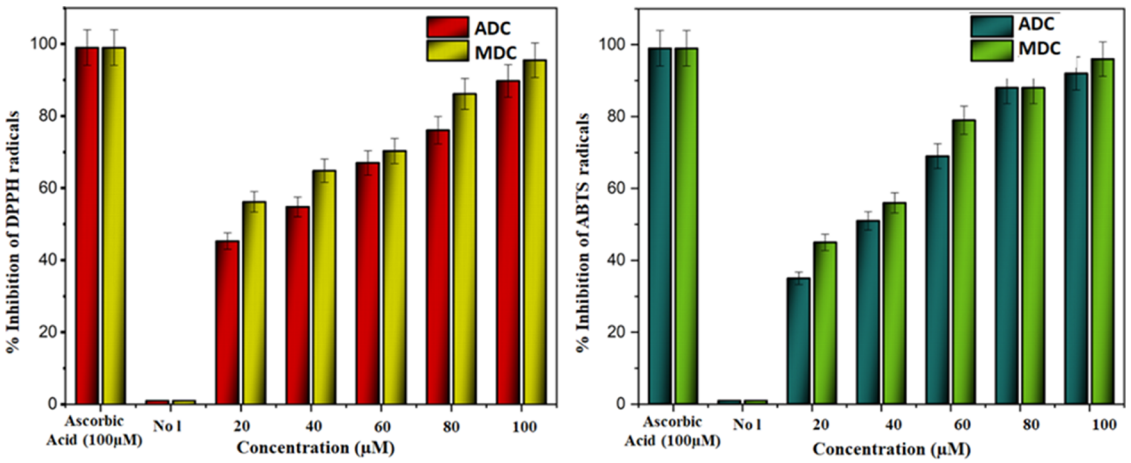

Figure 13. DPPH and ABTS antioxidant activities of compounds.

(Figure 11) diagram. Thus, MDC and ADC may easily form bonds and interact with biomolecules via hydrogen bonding.

3.6.3. Molecular Electrostatic Potential (MEP). DFT at the B3LYP/6-311G** level is used to calculate the theoretical MEP. Figure 12 shows the MEP surfaces of MDC and ADC. When evaluating how molecular interactions are directed, the MEP is used to forecast the nucleophilic and electrophilic centers in the molecule. The red area has a value of 6.784×10^{-2}, which indicates high electron density (nucleophilic); whereas, the blue zone has a value of -6.784×10^{-2}, which indicates low electron density (electrophilic) with a negative sign. White is a symbol of a neutral atom. MEP focuses in particular on the electrostatic environment, charge distribution, and potential for molecular interaction.

In MDC, the electron-rich nucleophilic center is located in the amide carbonyl and nitro groups. The electrophilic center is seen in amide nitrogen and methylene groups in the methylenedioxyphenyl ring. Similarly, for ADC, the nucleophilic center is in amide carbonyl, acetophenone carbonyl, and nitro groups. Electron deficiency is seen across the amide nitrogen and methylene groups in the methylenedioxyphenyl ring. We can foresee the groups that will readily interact with the macromolecules from the MEP results. Here, the macromolecules can bind with MDC and ADC via electron sharing through carbonyl and nitro groups. Amide nitrogen and methylene groups in the methylenedioxyphenyl ring can accept electrons from macromolecules and form bonds. Both MDC and ADC have the potential to engage with any target protein's active site. They are acceptable for use in medicinal chemistry.[93]

3.7. *In Vitro* and *Ex Vivo* Biological Studies. *3.7.1. In Vitro Antioxidant Assay.* In healthy human cells, unstable radicals have a propensity to form stable pairs with biological macromolecules like proteins. This leads to the damage to cells that are crucial in the development of cancer and heart diseases. The result of an oxidation process that takes place within the human body is the resulting free radicals. Antioxidants help in stopping cell deterioration by scavenging the free radicals that are created. The antioxidant activity of MDC and ADC is quantified by this study, and the inhibition percentage graph is plotted in Figure 13. The initial color of DPPH in ethanol is purple or violet, and we can see that the color fades to various shades of yellow when MDC and ADC are added. The amount of electrons increases and the discoloration turns yellow when an antioxidant adds a hydrogen atom to DPPH to form DPPH-H.[94] By using a similar method of action to acquire electrons from the antioxidant, the addition of antioxidant causes the color of the $ABTS^{\bullet+}$ solution to change from deep blue to colorless.[95] Ascorbic acid is used as the positive control. From DPPH and $ABTS^{\bullet+}$ scavenging assay results, the corresponding IC_{50} values for MDC and ADC are 25.28 ± 0.12, 55.05 ± 0.3 and 41.04 ± 0.25, 66.13 ± 0.34 μM, respectively; whereas ascorbic acid, a positive control, has IC_{50} values of 11.61 ± 0.31 and 11.26 ± 0.55 μM, respectively. The results of the antioxidant investigation demonstrate that MDC and ADC both effectively scavenge the free radicals present in the solution and exhibit a promising antioxidant activity when compared to the positive control. The DPPH and $ABTS^{\bullet+}$ acquire stability by taking electrons from MDC and ADC. From scientific literature,[96,97] the presence of a methoxy group, a +M substituted group in the para position, and a −M substitution in the meta position favor the antioxidant activity. The methoxy group, an electron donor with beneficial mesomeric action, is present in the core moiety of MDC in the para position. Both MDC and ADC exhibit good antioxidant properties, although MDC is a more powerful antioxidant when comparing IC_{50} values and SAR observations.

3.7.2. Ex Vivo Anti-inflammatory Activity. On investigating the hemolytic activity of MDC and ADC, the anti-inflammatory medicine aceclofenac exhibits an increase in activity with concentration, as shown in Figure 14. When red blood cells (RBCs) are added to the hypotonic solution, the hemoglobin begins to oxidize, which causes the RBC membrane to burst. Free radical production in ruptured cells is then sparked by lipid peroxidation. At a concentration of 20 mM, MDC and ADC demonstrated 55 and 51% anti-inflammatory action, respectively, and as the concentration increases, the activity likewise increases to 90 and 88%. The positive control has an IC_{50} value of 3.87 ± 0.28 μM, while MDC and ADC have values of 21.05 ± 0.10 and 27.54 ± 0.22 μM, respectively. The anti-inflammatory activity of both MDC and ADC is extremely good and promising, although ADC outperformed MDC in terms of IC_{50} values and the percentage of anti-inflammatory activity when compared with the industry standard.

3.7.3. In Vitro α-GD Inhibition Assay. Newly synthesized MDC and ADC are investigated for their ability to inhibit α-GD protein, and the results are compared with the positive control acarbose. The enzyme α-glucosidase will catalyze the

https://doi.org/10.1021/acsomega.3c07555
ACS Omega 2024, 9, 7850−7868

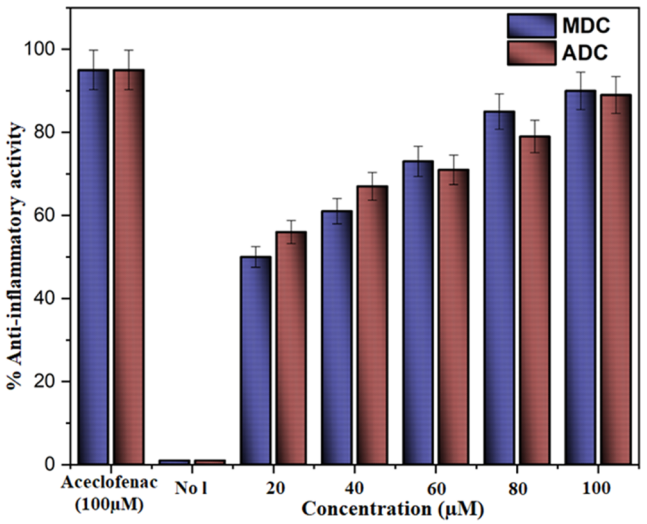

Figure 14. Anti-inflammatory activity of MDC and ADC.

transformation of the substrate 4-nitrophenyl-α-D-glucopyranoside into α-D-glucopyranoside and p-nitrophenol under the given experimental conditions (pH = 6.8; T = 37 °C). The latter product's yellow hue is spectrophotometrically evaluated at 405 nm, and the inhibition percentage graph is plotted in Figure 15. At a concentration of 10 mM, ADC and MDC

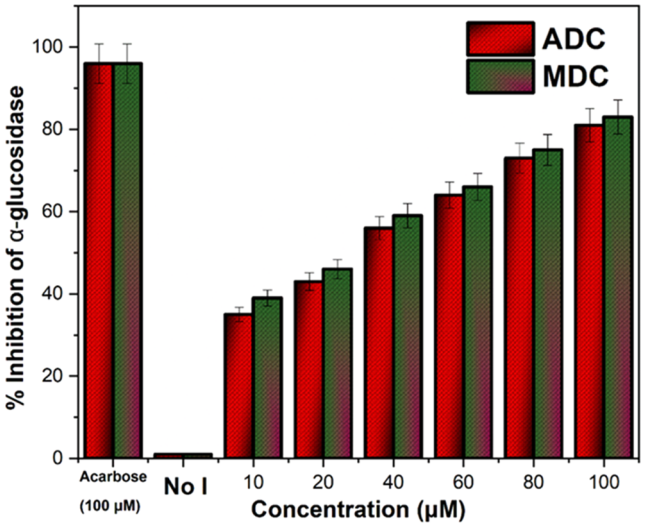

Figure 15. α-Glucosidase inhibition by MDC and ADC.

demonstrated 35 and 39% α-GD inhibition, respectively, and as the concentration increased, the activity was found to increase by 81 and 83%. The positive control has an IC_{50} value of 14.27 ± 0.21 μM, while ADC and MDC have values of 46.05 ± 0.10 and 41.11 ± 0.52 μM, respectively. Both MDC and ADC have the potential to inhibit α-GD; while considering IC_{50} values and comparison with the positive control, MDC is a better α-GD inhibitor.

3.7.4. In Vitro DPP-4 Inhibition Assay. The potential of MDC and ADC to inhibit DPP-4 is tested via fluorometric assay with sitagliptin as the positive control. The investigation involved monitoring the release of 7-amino-4-methylcoumarin (AMC), a fluorescent compound that is produced when DPP-4 cleaves H-Gly-Pro-7-amido-4-methylcoumarin hydrobromide (GP-AMC). The study is performed with 50, 100, 150, and 200 μM concentrations of MDC and ADC for 5−60 min after adding the inhibitor. The results are plotted in a line graph of time vs concentration, and the slope values for each concentration are calculated. Simultaneously, slope values are plotted for sitagliptin and the blank solution (without inhibitor). The slope values calculated from the line graph are utilized to calculate the percentage of inhibition, as shown Figure 16. The IC_{50} value was calculated by plotting the

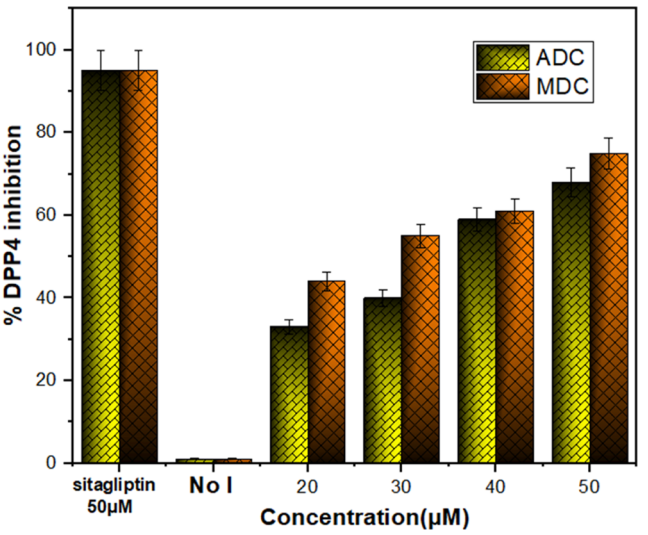

Figure 16. Dipeptidyl peptidase-4 inhibition by MDC and ADC.

percentage of inhibition versus different concentrations of MDC and ADC. A similar process was employed for the positive control. The IC_{50} value for sitagliptin is 3.88 ± 0.23 μM and that for ADC and MDC is 31.02 ± 0.17 and 25.34 ± 0.11 μM, respectively. MDC and ADC moderately inhibit DPP-4, and MDC with less IC_{50} value upon comparing ADC exhibits better inhibition.

3.7.5. In Vitro MPO Inhibition Assay. MPO inhibition is carried out in a cell-free system by utilizing 3,5,3′,5′-tetramethylbenzidine (TMB) as an enzyme substrate and salicylhydroxamic acid as a positive control. Percentage of inhibition vs absorbance is plotted with varying concentrations of MDC and ADC, and the IC_{50} values are then calculated. The positive control has an IC_{50} value of 2.9 ± 0.13 μM, while MDC and ADC have values of 4.5 ± 0.19 and 10 ± 0.27 μM, respectively. At low concentrations (5 μM), MDC exhibits more than 50% inhibition. Even though we achieved 50% inhibition at low concentration, we still wanted to evaluate the maximum inhibition. At 25 μM, it exhibits a maximal inhibition that is more similar to the positive control. From the percentage inhibition graph in Figure 17 and the IC_{50} value in Table 10, MDC exhibited good inhibition at very low concentrations.

Upon comparison of IC_{50} values of MDC and ADC with α-GD, DPP-4, and MPO (Table 10), MDC exhibited selective MPO inhibition with an IC_{50} value closer to the positive control. Docking results put forward that MDC has good interaction with the MPO protein's active site pockets. This makes it easier for MDC to dock with a protein and stop it from acting. Results from theoretical molecular docking and experimental *in vitro* studies of MDC are in good agreement with one another. In light of the performed studies, we strongly

https://doi.org/10.1021/acsomega.3c07555
ACS Omega 2024, 9, 7850−7868

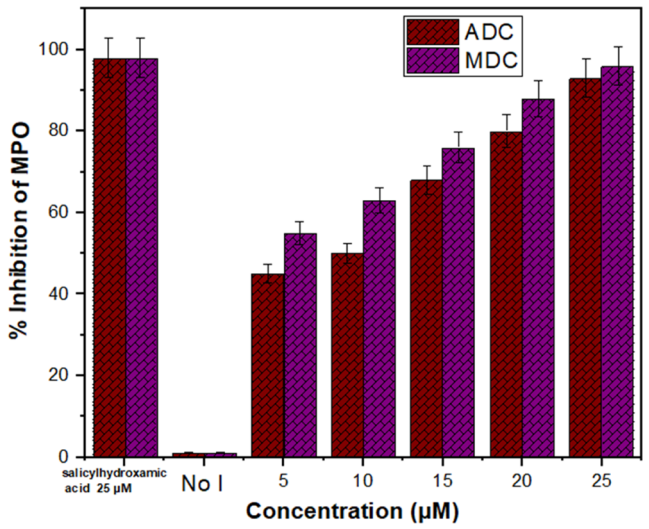

Figure 17. Myeloperoxidase inhibition by MDC and ADC.

Table 10. IC_{50} Values for MDC, ADC, and Positive Control with α-GD, DPP-4, and MPO

protein	ligand	IC_{50} (μM)
α-GD	acarbose	14.27 ± 0.21
	MDC	41.11 ± 0.52
	ADC	46.05 ± 0.10
DPP-4	sitagliptin	3.88 ± 0.23
	MDC	25.34 ± 0.11
	ADC	31.02 ± 0.17
MPO	salicylhydroxamic acid	2.9 ± 0.13
	MDC	4.5 ± 0.19
	ADC	10 ± 0.27

recommend MDC for MPO inhibition after performing *in vivo* studies.

4. CONCLUSIONS

The findings of the current study suggest that theoretical and experimental biological studies using synthesized derivatives of 6-nitrobenzo-[1,3]-dioxole-5-carboxamide yield promising results. Molecular docking, ADMET, and Lipinski rules opine that the compounds are similar to drugs and the ligands exhibit strong protein-binding interactions. The ligands exhibit good binding energy to MPO and are selective for the oxidative protein. MDC exhibited more activity than ADC in anti-inflammatory and antioxidant studies. SC-XRD analysis revealed the precise structural characteristics of the compounds. The experimental (SC-XRD) and theoretical (DFT) measurements of MDC and ADC bond lengths are consistent. Molecules' chemical behavior is predicted using DFT calculations, and a smaller energy gap from FMO revealed that these molecules are very interactive. Methylenedioxyphenyl ring and the amide group in both FMO and MEP molecules are capable of easy interaction and binding with the active sites of proteins or other biomolecules. The *in vitro* α-GD, DPP-4, and MPO inhibition by both MDC and ADC appeared to be promising. MDC outperformed ADC in terms of IC_{50} values and the percentage of inhibition activity when compared with the positive control. MDC's overall bioactivity is favored by the inclusion of an electron-donating group, methoxy group, in the para position, providing appropriate geometrical properties to the molecules. This offers avenues for MDC to fit into the target protein intact. In view of this proper geometrical orientation, MDC exhibits selective myeloperoxidase inhibition in *in vitro* enzymatic studies. Therefore, for the development of myeloperoxidase-targeted medicines for cardiovascular disease, derivatives of 6-nitrobenzo[1,3]-dioxole-5-carboxamide, which have not yet been identified in the literature, are ideal.

■ ASSOCIATED CONTENT

Supporting Information

The Supporting Information is available free of charge at https://pubs.acs.org/doi/10.1021/acsomega.3c07555.

Synthesis and crystallization; characterization data for synthesized derivatives and starting material; crystal structure report for MDC and ADC; procedures for *in vitro* and *ex vivo* biological studies (PDF)

■ AUTHOR INFORMATION

Corresponding Author

Rajagopal Desikan − *Department of Chemistry, School of Advanced Sciences, Vellore Institute of Technology, Vellore 632014 Tamilnadu, India;* orcid.org/0000-0002-6118-8823; Email: desikanrajagopal@gmail.com

Authors

Reshma Rajan − *Department of Chemistry, School of Advanced Sciences, Vellore Institute of Technology, Vellore 632014 Tamilnadu, India*

Sambantham Karthikeyan − *Department of Chemistry, School of Advanced Sciences, Vellore Institute of Technology, Vellore 632014 Tamilnadu, India;* orcid.org/0000-0001-7807-151X

Complete contact information is available at: https://pubs.acs.org/10.1021/acsomega.3c07555

Notes

The authors declare no competing financial interest.

■ ACKNOWLEDGMENTS

The authors are grateful to VIT-RGEMS for the financial support. They also thank DST-VIT-FIST for NMR and single-crystal XRD, VIT-SIF for FT-IR, and VIT for HRMS and other instrumentation facilities.

■ REFERENCES

(1) Tributino, J.-L.; Duarte, C.-D.; Corrêa, R.-S.; Doriguetto, A.-C.; Ellena, J.; Romeiro, N.-C.; Castro, N.-G.; Miranda, A.-L.; Barreiro, E.-J.; Fraga, C.-A. Novel 6-methanesulfonamide-3, 4-methylenedioxyphenyl-N-acylhydrazones: Orally effective anti-inflammatory drug candidates. *Bioorg. Med. Chem.* **2009**, *17* (3), 1125−1131.

(2) Rehman, A.; Siddiqa, A.; Abbasi, M.-A.; Rasool, S.; Siddiqui, S.-Z.; Ahmad, I.; Afzal, S. Synthesis of some new 5-substituted-2-((6-chloro-3, 4-methylenedioxyphenyl) methylthio)-1, 3, 4-Oxadiazole derivatives as suitable antibacterial inhibitors. *Bull. Fac. Pharm.* **2015**, *53* (1), 37−43.

(3) Islam, M.-T.; Hasan, J.; Snigdha, H.-S.; Ali, E.-S.; Sharifi-Rad, J.; Martorell, M.; Mubarak, M.-S. Chemical profile, traditional uses, and biological activities of Piper chaba Hunter: A review. *J. Ethnopharmacol.* **2020**, *257*, No. 112853.

(4) Yadav, V.; Krishnan, A.; Vohora, D. A systematic review on Piper longum L.: Bridging traditional knowledge and pharmacological evidence for future translational research. *J. Ethnopharmacol.* **2020**, *247*, No. 112255.

(5) Jayaraj, P.; Sarkar, P.; Routh, S.; Sarathe, C.; Desikan, R.; Thirumurugan, K. A promising discovery of an anti-aging chemical conjugate derived from lipoic acid and sesamol established in Drosophila melanogaster. *New J. Chem.* **2022**, *46* (23), 11229−11241.
(6) Ying, Z.; Desikan, R.; Xu, X.; Maiseyeu, A.; Liu, C.; Sun, Q.; Ziouzenkova, O.; Parthasarathy, S.; Rajagopalan, S. Modified methylenedioxyphenol analogs lower LDL cholesterol through induction of LDL receptor expression. *J. Lipid Res.* **2012**, *53* (5), 879−887.
(7) Kesarwani, K.; Gupta, R. Bioavailability enhancers of herbal origin: An overview. *Asian Pac. J. Trop. Biomed.* **2013**, *3* (4), 253−266.
(8) Friedemann, T.; Schumacher, U.; Tao, Y.; Leung, A.-K.; Schröder, S. Neuroprotective activity of coptisine from Coptis chinensis (Franch). *eCAM* **2015**, *2015*, No. 827308.
(9) Andargie, M.; Vinas, M.; Rathgeb, A.; Möller, E.; Karlovsky, P. Lignans of sesame (Sesamum indicum L.): a comprehensive review. *Molecules* **2021**, *26* (4), No. 883.
(10) Kasibhatta, R.; Naidu, M.-U. R. Influence of piperine on the pharmacokinetics of nevirapine under fasting conditions: a randomised, crossover, placebo-controlled study. *Drugs R&D* **2007**, *8*, 383−391.
(11) Singh, S.; Kumar, P. Piperine in combination with quercetin halt 6-OHDA induced neurodegeneration in experimental rats: Biochemical and neurochemical evidences. *Neurosci. Res.* **2018**, *133*, 38−47.
(12) Johnson, J.-J.; Nihal, M.; Siddiqui, I.-A.; Scarlett, C.-O.; Bailey, H.-H.; Mukhtar, H.; Ahmad, N. Enhancing the bioavailability of resveratrol by combining it with piperine. *Mol. Nutr. Food Res.* **2011**, *55* (8), 1169−1176.
(13) Rascol, O.; Dubois, B.; Caldas, A.-C.; Senn, S.; Del Signore, S.; Lees, A. Early piribedil monotherapy of Parkinson's disease: A planned seven-month report of the REGAIN study. *Mov. Disord.* **2006**, *21* (12), 2110−2115.
(14) Yin, J.; Xing, H.; Ye, J. Efficacy of berberine in patients with type 2 diabetes. *Metabolism* **2008**, *57* (5), 712−717.
(15) Balestrini, S.; Doccini, V.; Boncristiano, A.; Lenge, M.; De Masi, S.; Guerrini, R. Efficacy and safety of long-term treatment with stiripentol in children and adults with drug-resistant epilepsies: a retrospective cohort study of 196 patients. *Drugs-Real World Outcomes* **2022**, *9* (3), 451−461.
(16) Maigaard, S.; Frimodt-Möller, N.; Welling, P.-G.; Madsen, P.-O. Cinoxacin: pharmacokinetics and tolerance in patients with normal and impaired renal function. *Antimicrob. Agents Chemother.* **1979**, *16* (3), 411−416.
(17) Jayaraj, P.; Narasimhulu, C. A.; Rajagopalan, S.; Parthasarathy, S.; Desikan, R. Sesamol: a powerful functional food ingredient from sesame oil for cardioprotection. *Food Funct.* **2020**, *11* (2), 1198−1210.
(18) Almadiy, A. A.; Al-Ghamdi, M. S.; Al-Akeel, R. K.; Soliman, M. M.; Ali, M. M. Qualitative structure-activity relationships of aryl isoprenoid derivatives as biorational juvenoids-reweighing. *Int. J. Trop. Insect Sci.* **2023**, *43* (3), 1111−1121.
(19) Ying, Z.; Chen, M.; Xie, X.; Wang, X.; Kherada, N.; Desikan, R.; Mihai, G.; Burns, P.; Sun, Q.; Rajagopalan, S. Lipoicmethylenedioxyphenol Reduces Experimental Atherosclerosis through Activation of Nrf2 Signaling. *PLoS One* **2016**, *11* (2), No. e0148305.
(20) Yang, H.; Du, Z.; Wang, W.; Song, M.; Sanidad, K.; Sukamtoh, E.; Zhang, G.; et al. Structure−activity relationship of curcumin: Role of the methoxy group in anti-inflammatory and anticolitis effects of curcumin. *J. Agric. Food Chem.* **2017**, *65* (22), 4509−4515.
(21) Scozzafava, A.; Passaponti, M.; Supuran, C. T.; Gülçin, İ. Carbonic anhydrase inhibitors: guaiacol and catechol derivatives effectively inhibit certain human carbonic anhydrase isoenzymes (hCA I, II, IX and XII). *J. Enzyme Inhib. Med. Chem.* **2015**, *30* (4), 586−591.
(22) Walle, T. Methoxylated flavones, a superior cancer chemopreventive flavonoid subclass? *Semin. Cancer Biol.* **2007**, *17* (5), 354−362.
(23) Meltzer, P. C.; Butler, D.; Deschamps, J. R.; Madras, B. K. 1-(4-Methylphenyl)-2-pyrrolidin−1-yl-pentan−1-one (Pyrovalerone) analogues: a promising class of monoamine uptake inhibitors. *J. Med. Chem.* **2006**, *49* (4), 1420−1432.
(24) Foley, K. F.; DeSanty, K. P.; Kast, R. E. Bupropion: pharmacology and therapeutic applications. *Expert Rev. Neurother.* **2006**, *6* (9), 1249−1265.
(25) Sumalatha, Y.; Reddy, T. R.; Reddy, P. P.; Satyanarayana, B. A simple, efficient and scalable synthesis of hypnotic agent, zolpidem. *ARKIVOC* **2009**, *2*, 315−320.
(26) Zubkov, F. I.; Kouznetsov, V. V. Traveling across Life Sciences with Acetophenone—A Simple Ketone That Has Special Multipurpose Missions. *Molecules* **2023**, *28* (1), No. 370.
(27) Jayaraj, P.; Narasimhulu, C. A.; Maiseyeu, A.; Durairaj, R.; Rao, S.; Rajagopalan, S.; Parthasarathy, S.; Desikan, R. Methoxyphenol derivatives as reversible inhibitors of myeloperoxidase as potential antiatherosclerotic agents. *Future Med. Chem.* **2020**, *12* (2), 95−110.
(28) Meng, W.; Brigance, R. P.; Chao, H.-J.; Fura, A.; Harrity, T.; Marcinkeviciene, J.; O'Connor, S. P.; Tamura, J. K.; Xie, D.; Zhang, Y.; Klei, H. E.; et al. Discovery of 6-(Aminomethyl)-5-(2, 4-dichlorophenyl)-7-methylimidazo [1, 2-a] pyrimidine-2-carboxamides as Potent, Selective Dipeptidyl Peptidase-4 (DPP4) Inhibitors. *J. Med. Chem.* **2010**, *53* (15), 5620−5628.
(29) Avula, S.-K.; Ullah, S.; Halim, S.-A.; Khan, A.; Anwar, M.-U.; Csuk, R.; Al-Harrasi, A.; Rostami, A. Meldrum-Based-1 H-1, 2, 3-Triazoles as Antidiabetic Agents: Synthesis, In Vitro α-Glucosidase Inhibition Activity, Molecular Docking Studies, and In Silico Approach. *ACS Omega* **2023**, *8* (28), 24901−24911.
(30) Poznyak, A.; Grechko, A. V.; Poggio, P.; Myasoedova, V. A.; Alfieri, V.; Orekhov, A. N. The Diabetes Mellitus-Atherosclerosis Connection: The Role of Lipid and Glucose Metabolism and Chronic Inflammation. *Int. J. Mol. Sci.* **2020**, *21* (5), No. 1835.
(31) Avagimyan, A.; Fogacci, F.; Pogosova, N.; Kakrurskiy, L.; Kogan, E.; Urazova, O.; Sarrafzadegan, N.; et al. Diabetic cardiomyopathy: 2023 update by the international multidisciplinary board of experts. *Curr. Probl. Cardiol.* **2023**, *49* (1 Pt A), No. 102052.
(32) Tsalamandris, S.; Antonopoulos, A.-S.; Oikonomou, E.; Papamikroulis, G.-A.; Vogiatzi, G.; Papaioannou, S.; Deftereos, S.; Tousoulis, D. The Role of Inflammation in Diabetes: Current Concepts and Future Perspectives. *Eur. Cardiol.* **2019**, *14* (1), 50−59.
(33) Frangie, C.; Daher, J. Role of myeloperoxidase in inflammation and atherosclerosis (Review). *Biomed. Rep.* **2022**, *16* (6), No. 53.
(34) Johnström, P.; Bergman, L.; Varnas, K.; Malmquist, J.; Halldin, C.; Farde, L. Development of rapid multistep carbon-11 radiosynthesis of the myeloperoxidase inhibitor AZD3241 to assess brain exposure by PET microdosing. *Nucl. Med. Biol.* **2015**, *42* (6), 555−560.
(35) Patnaik, A.; Axford, L.; Deng, L.; Cohick, E.; Ren, X.; Loi, S.; Kecman, S.; Hollis-Symynkywicz, M.; Harrison, T. J.; Papillon, J. P. N.; Dales, N.; Hamann, L. G.; Lee, L.; Regard, J. B.; Marcinkeviciene, J.; Marro, M. L.; Patterson, A. W. Discovery of a novel indole pharmacophore for the irreversible inhibition of myeloperoxidase (MPO). *Bioorg. Med. Chem.* **2020**, *28* (12), No. 115548.
(36) Li, S. C.; Jhang, W. F.; Liou, T. J.; Yang, D. Y. Photochemical synthesis of indazolo [3, 2-b] quinazolines and their redox-switching properties. *Dyes Pigm.* **2015**, *114*, 259−266.
(37) Wang, T.; Dong, Y.; Wang, L. C.; Xiang, B. R.; Chen, Z.; Qu, L. B. Design, synthesis and structure-activity relationship studies of 6-phenyl-4, 5-dihydro-3 (2H)-pyridazinone derivatives as cardiotonic agents. *Arzneim. Forsch.* **2008**, *58* (11), 569−573.
(38) Ali, S.; Ali, M.; Khan, A.; Ullah, S.; Waqas, M.; Al-Harrasi, A.; Saadiq, M.; et al. Novel 5-(Arylideneamino)-1 H-Benzo [d] imidazole-2-thiols as Potent Anti-Diabetic Agents: Synthesis, In Vitro α-Glucosidase Inhibition, and Molecular Docking Studies. *ACS Omega* **2022**, *7* (48), 43468−43479.
(39) Singh, A.; Singh, K.; Sharma, A.; Kaur, K.; Kaur, K.; Chadha, R.; Bedi, P. M. S. Recent developments in synthetic α-glucosidase inhibitors: A comprehensive review with structural and molecular insight. *J. Mol. Struct.* **2023**, *1281*, No. 135115.

https://doi.org/10.1021/acsomega.3c07555
ACS Omega 2024, 9, 7850−7868

(40) Molinaro, A.; Nemet, I.; Bel Lassen, P.; Chakaroun, R.; Nielsen, T.; Aron-Wisnewsky, J.; Bäckhed, F.; et al. Microbially produced imidazole propionate is associated with heart failure and mortality. *Heart Failure* **2023**, *11* (7), 810−821.
(41) Dianat, S.; Moghimi, S.; Mahdavi, M.; Nadri, H.; Moradi, A.; Firoozpour, L.; Foroumadi, A.; et al. Quinoline-based imidazole-fused heterocycles as new inhibitors of 15-lipoxygenase. *J. Enzyme Inhib. Med. Chem.* **2016**, *31* (Suppl. 3), 205−209.
(42) Kanso, F.; Khalil, A.; Noureddine, H.; El-Makhour, Y. Therapeutic perspective of thiosemicarbazones derivatives in inflammatory pathologies: A summary of in vitro/in vivo studies. *Int. Immunopharmacol.* **2021**, *96*, No. 107778.
(43) Iqbal, S.; Khan, M. A.; Jabeen, A.; Yousuf, S.; Zafar, F.; Batool, F.; Ganatra, M. U.; Basha, F. Z. Synthesis, crystal structure, and reactive oxygen species (ROS) inhibition of N− and O−linked triazole analogues of harmine. *J. Mol. Struct.* **2022**, *1261*, No. 132796.
(44) Macalalad, M. A. B.; Gonzales, A. A., III In Silico Screening and Identification of Antidiabetic Inhibitors Sourced from Phytochemicals of Philippine Plants against Four Protein Targets of Diabetes (PTP1B, DPP-4, SGLT-2, and FBPase). *Molecules* **2023**, *28* (14), No. 5301.
(45) Ying, Z.; Kherada, N.; Kampfrath, T.; Mihai, G.; Simonetti, O.; Desikan, R.; Rajagopalan, S.; et al. A modified sesamol derivative inhibits progression of atherosclerosis. *Arterioscler., Thromb., Vasc. Biol.* **2011**, *31* (3), 536−542.
(46) VanGilder, R. L.; Huber, J. D. Sesamol: A treatment for diabetes-associated blood-brain barrier dysfunction. *Postdoc J.* **2014**, *2* (7), 13−22.
(47) Daina, A.; Michielin, O.; Zoete, V. SwissADME: a free web tool to evaluate pharmacokinetics, drug-likeness and medicinal chemistry friendliness of small molecules. *Sci. Rep.* **2017**, *7* (1), No. 42717.
(48) Pires, D. E. V.; Blundell, T.-L.; Ascher, D.-B. pkCSM: predicting small-molecule pharmacokinetic and toxicity properties using graph-based signatures. *J. Med. Chem.* **2015**, *58* (9), 4066−4072.
(49) Banerjee, P.; Eckert, A. O.; Schrey, A.-K.; Preissner, R. ProTox-II: a webserver for the prediction of toxicity of chemicals. *Nucleic Acids Res.* **2018**, *46* (W1), W257−W263.
(50) Jayaraj, P.; Shavi, G. V.; Srinivasan, A. K.; Raghavendra, R.; Sivaramakrishna, A.; Desikan, R. A pre-formulation strategy for the liposome encapsulation of new thioctic acid conjugates for enhanced chemical stability and use as an efficient drug carrier for MPO-mediated atherosclerotic CVD treatment. *New J. Chem.* **2020**, *44* (7), 2755−2767.
(51) Corredor, J.-D.; Febres-Molina, C.; Jaña, G.-A.; Jiménez, V.-A. Insight into the Role of Active Site Protonation States and Water Molecules in the Catalytic Inhibition of DPP4 by Vildagliptin. *J. Chem. Inf. Model.* **2023**, *63* (4), 1338−1350.
(52) Yamamoto, K.; Miyake, H.; Kusunoki, M.; Osaki, S. Crystal structures of isomaltase from Saccharomyces cerevisiae and in complex with its competitive inhibitor maltose. *FEBS J.* **2010**, *277* (20), 4205−4214.
(53) Sedelmeier, J.; Ley, S. V.; Baxendale, I. R.; Baumann, M. $KMnO_4$-mediated oxidation as a continuous flow process. *Org. Lett.* **2010**, *12* (16), 3618−3621.
(54) Bao, Y.; Deng, Z.; Feng, J.; Zhu, W.; Li, J.; Wan, J.; Liu, G. A B2 (OH) 4-Mediated Synthesis of 2-Substituted Indazolone and Its Application in a DNA-Encoded Library. *Org. Lett.* **2020**, *22* (16), 6277−6282.
(55) Chen, Y.; Liu, X.; Shi, W.; Zheng, S.; Wang, G.; He, L. One-Pot Synthesis of Seven-Membered Heterocyclic Derivatives of Diazepines Involving Copper-Catalyzed Rearrangement Cascade Allyl-Amination. *J. Org. Chem.* **2020**, *85* (8), 5146−5157.
(56) Jayaraj, P.; Desikan, R. Design, Synthesis, and Preclinical Bio Evaluation of Chemical Conjugates Derived from Phytophenols and Nitrobenzoate as First Plausible Inhibitors of MPO Useful in CVD Treatment. *Biointerface Res. Appl. Chem.* **2021**, *11* (4), 11630−11652.
(57) Reddy Manne, M.; Panicker, R.-R.; Ramakrishnan, K.; Hareendran, H.-M.; Kumar Pal, S.; Kumar, S.; Pallepogu, R.; Desikan, R.; Sivaramakrishna, A. Synthesis and Biological Evaluation of a Series of Quinoline-Based Quinazolinones and Carbamic Anhydride Derivatives. *ChemistrySelect* **2023**, *8* (3), No. e202204508.
(58) Yousefnejad, F.; Mohammadi-Moghadam-Goozali, M.; Sayahi, M. H.; Halimi, M.; Moazzam, A.; Mohammadi-Khanaposhtani, M.; Mahdavi, M.; et al. Design, synthesis, in vitro, and in silico evaluations of benzo [d] imidazole-amide−1, 2, 3-triazole-N-arylacetamide hybrids as new antidiabetic agents targeting α-glucosidase. *Sci. Rep.* **2023**, *13* (1), No. 12397.
(59) Proença, C.; Freitas, M.; Ribeiro, D.; Tomé, S. M.; Araújo, A. N.; Silva, A. M.; Fernandes, E.; Fernandes, E. The dipeptidyl peptidase-4 inhibitory effect of flavonoids is hindered in protein rich environments. *Food Funct.* **2019**, *10* (9), 5718−5731.
(60) Jayaraj, P.; Parthasarathy, S.; Rajagopalan, S.; Aluganti, C.; Desikan, R. Discovery of novel synthetic guaiacol derivatives as promising myeloperoxidase inhibitors (MPOIs) targeting atherosclerotic CVD. *ChemMedChem* **2020**, *15* (13), 1187−1199.
(61) Lipinski, C. A.; Lombardo, F.; Dominy, B. W.; Feeney, P. J. Experimental and computational approaches to estimate solubility and permeability in drug discovery and development settings. *Adv. Drug Delivery Rev.* **1997**, *23* (1−3), 3−25.
(62) Lipinski, C. A. Lead-and drug-like compounds: the rule-of-five revolution. *Drug Discovery Today: Technol.* **2004**, *1* (4), 337−341.
(63) Begaum, K. P.; Prabhu, T.; Kaleeswaran, S.; Kadaikunnan, S.; Abbas, G.; Muthu, S.; Dege, N.; et al. Synthesis, crystal structure, static and dynamic properties, molecular structure, reactive sites, wavefunction and molecular docking of 1-(3-((4-(diethylamino)-2-hydroxybenzylidene) amino) phenyl) ethan−1-one. *J. Mol. Struct.* **2023**, *1294*, No. 136348.
(64) Ghose, A. K.; Viswanadhan, V. N.; Wendoloski, J. J. A knowledge-based approach in designing combinatorial or medicinal chemistry libraries for drug discovery. 1. A qualitative and quantitative characterization of known drug databases. *J. Comb. Chem.* **1999**, *1* (1), 55−68.
(65) Veber, D. F.; Johnson, S. R.; Cheng, H. Y.; Smith, B. R.; Ward, K. W.; Kopple, K. D. Molecular properties that influence the oral bioavailability of drug candidates. *J. Med. Chem.* **2002**, *45* (12), 2615−2623.
(66) Egan, W. J.; Merz, K. M.; Baldwin, J. J. Prediction of drug absorption using multivariate statistics. *J. Med. Chem.* **2000**, *43* (21), 3867−3877.
(67) Muegge, I.; Heald, S. L.; Brittelli, D. Simple selection criteria for drug-like chemical matter. *J. Med. Chem.* **2001**, *44* (12), 1841−1846.
(68) Prasanna, S.; Doerksen, R. J. Topological polar surface area: a useful descriptor in 2D-QSAR. *Curr. Med. Chem.* **2009**, *16* (1), 21−41.
(69) Martin, Y. C. A bioavailability score. *J. Med. Chem.* **2005**, *48* (9), 3164−3170.
(70) Subramaniyan, R.; Ramarajan, R.; Ramalingam, A.; Sambandam, S.; Petersamy, A.; Guerroudj, A. R.; Boukabcha, N.; Chouaih, A. Microwave assisted synthesis, vibrational spectra, Hirshfeld surface and interaction energy, DFT, topology, in silico ADMET and molecular docking studies of 1, 2-bis (4-methoxybenzylidene) hydrazine. *J. Mol. Struct.* **2023**, *1278*, No. 134946.
(71) Patel, S.-G.; González-Bakker, A.; Vala, R.-M.; Patel, P.-J.; Puerta, A.; Malik, A.; Sharma, R.-K.; Padrón, J.-M.; Patel, H.-M. Microwave-assisted multicomponent synthesis of antiproliferative 2, 4-di.methoxy-tetrahydropyrimido [4, 5-b] quinolin-6 (7 H)-ones. *RSC Adv.* **2022**, *12* (47), 30404−30415.
(72) Pires, D. E. V.; Blundell, T.-L.; Ascher, D. B. pkCSM Predicting Small-Molecule Pharmacokinetic and Toxicity Properties Using Graph-Based Signatures. *J. Med. Chem.* **2015**, *58*, 4066−4072.
(73) Yeşilkaynak, T.; Özkömeç, F.-N.; Çeşme, M.; Demirdöğen, R.-E.; Sezer, C.-V.; Kutlu, H.-M.; Emen, F.-M. Novel thiourea derivative compounds: Thermal behavior, biological evaluation, Hirshfeld surfaces and frontier orbitals analyses, in silico ADMET profiling and molecular docking studies. *J. Mol. Struct.* **2023**, *1280*, No. 135086.

https://doi.org/10.1021/acsomega.3c07555
ACS Omega 2024, 9, 7850−7868

(74) Han, Y.; Zhang, J.; Hu, C.-Q.; Zhang, X.; Ma, B.; Zhang, P. In silico ADME and toxicity prediction of ceftazidime and its impurities. *Front. Pharmacol.* **2019**, *10*, No. 434.
(75) Esmaili, S.; Ebadi, A.; Khazaei, A.; Ghorbani, H.; Faramarzi, M.-A.; Mojtabavi, S.; Mahdavi, M.; Najafi, Z. Novel Pyrano [3, 2-c] quinoline−1,2,3-triazole Hybrids as Potential Anti-Diabetic Agents: In Vitro α-Glucosidase Inhibition, Kinetic, and Molecular Dynamics Simulation. *ACS Omega* **2023**, *8* (26), 23412−23424.
(76) Bauzá, A.; Frontera, A.; Mooibroek, T. J. π-Hole Interactions Involving Nitro Aromatic Ligands in Protein Structures. *Chem. - Eur. J.* **2019**, *25* (58), 13436−13443.
(77) Kumari, S.; Carmona, A. V.; Tiwari, A. K.; Trippier, P. C. Amide bond bioisosteres: Strategies, synthesis, and successes. *J. Med. Chem.* **2020**, *63* (21), 12290−12358.
(78) Trabbic, C. J.; George, S. M.; Alexander, E. M.; Du, S.; Offenbacher, J. M.; Crissman, E. J.; Erhardt, P. W.; et al. Synthesis and biological evaluation of isomeric methoxy substitutions on anti-cancer indolyl-pyridinyl-propenones: Effects on potency and mode of activity. *Eur. J. Med. Chem.* **2016**, *122*, 79−91.
(79) Fragopoulou, E.; Gkotsi, K.; Petsini, F.; Gioti, K.; Kalampaliki, A. D.; Lambrinidis, G.; Kostakis, I. K.; Tenta, R. Synthesis and Biological Evaluation of Resveratrol Methoxy Derivatives. *Molecules* **2023**, *28* (14), No. 5547.
(80) Kruve, A.; Kaupmees, K. Adduct formation in ESI/MS by mobile phase additives. *J. Am. Soc. Mass Spectrom.* **2017**, *28* (5), 887−894.
(81) Lakhera, S.; Devlal, K.; Rana, M.; Kanagathara, N.; Dhanusha, A.; Girisun, T. S.; Chowdhury, P. Two-photon absorption and optical limiting in 7-diethylamino-4-methyl coumarin. *J. Photochem. Photobiol., A* **2023**, *447*, No. 115216.
(82) Prabavathi, N.; Nilufer, A.; Krishnakumar, V. Spectroscopic (FT-IR, FT-Raman, UV and NMR) investigation, conformational stability, NLO properties, HOMO-LUMO and NBO analysis of hydroxyquinoline derivatives by density functional theory calculations. *Spectrochim. Acta, Part A* **2013**, *114*, 449−474.
(83) Pearson, R. G. Chemical hardness and density functional theory. *J. Chem. Sci.* **2005**, *117*, 369−377.
(84) Pandey, N.; Mehata, M. S.; Pant, S.; Tewari, N. Structural, electronic and NLO properties of 6-aminoquinoline: a DFT/TD-DFT study. *J. Fluoresc.* **2021**, *31* (6), 1719−1729.
(85) Koopmans, T. über Die Zuordnung Von Wellenfunktionen Und Eigenwerten Zu Den Einzelnen Elektronen Eines Atoms. *Physica* **1934**, *1*, 104−113.
(86) Parr, R. G.; Szentpály, L. V.; Liu, S. Electrophilicity index. *J. Am. Chem. Soc.* **1999**, *121* (9), 1922−1924.
(87) Haroon, M.; Akhtar, T.; Shaikh, Q.-U.; Mehmood, H.; Khalid, M.; Asghar, M.-A.; Alshehri, S.-M.; Ojha, S.-C. Facile Synthesis and DFT Analysis of Novel Thiazole-Based Hydrazones: An Experimental and Theoretical Perspective. *ACS Omega* **2023**, *8* (30), 27488−27499.
(88) Pasuparthy, S.-D.; Maiti, B. [CMMIM][BF4−] Ionic Liquid-Catalyzed Facile, One-Pot Synthesis of Chromeno [4, 3-d] pyrido [1, 2-a] pyrimidin−6-ones: Evaluation of Their Photophysical Properties and Theoretical Calculations. *ACS Omega* **2022**, *7* (43), 39147−39158.
(89) Spackman, M.-A.; Jayatilaka, D. Hirshfeld surface analysis. *CrystEngComm* **2009**, *11* (1), 19−32.
(90) Ahmed, M. N.; Ghias, M.; Shah, S.-W.-A.; Shoaib, M.; Tahir, M.-N.; Ashfaq, M.; Ibrahim, M. A.; Andleeb, H.; Gil, D.-M.; Frontera, A. X-ray characterization, Hirshfeld surface analysis, DFT calculations, in vitro and in silico lipoxygenase inhibition (LOX) studies of dichlorophenyl substituted 3-hydroxy-chromenones. *New J. Chem.* **2021**, *45* (42), 19928−19940.
(91) Azouzi, K.; Hamdi, B.; Zouari, R.; Salah, A.-B. Synthesis, structure and Hirshfeld surface analysis, vibrational and DFT investigation of (4-pyridine carboxylic acid) tetrachlorocuprate (II) monohydrate. *Bull. Mater. Sci.* **2017**, *40*, 289−299.
(92) Demircioğlu, Z.; Ersanli, C.-C.; Kaya kantar, G.; Şaşmaz, S. Spectroscopic, Hirshfeld surface, X-ray diffraction methodologies and local & global chemical activity calculations of 5-(2-methoxy-4-(prop-1-en-1-yl) phenoxy) pyrazine-2, 3-dicarbonitrile. *J. Mol. Struct.* **2019**, *1181*, 25−37.
(93) Jayaraj, P.; Desikan, R. Synthesis, crystal structure, and DFT calculations of 2H-1, 3-benzodioxol-5-yl 3-(4-hydroxy-3-methoxyphenyl) prop-2-enoate. *Chem. Data Collect.* **2020**, *29*, No. 100518.
(94) Baliyan, S.; Mukherjee, R.; Priyadarshini, A.; Vibhuti, A.; Gupta, A.; Pandey, R.-P.; Chang, C.-M. Determination of antioxidants by DPPH radical scavenging activity and quantitative phytochemical analysis of Ficus religiosa. *Molecules* **2022**, *27* (4), No. 1326.
(95) Ilyasov, I. R.; Beloborodov, V.-L.; Selivanova, I.-A.; Terekhov, R.-P. ABTS/PP decolorization assay of antioxidant capacity reaction pathways. *Int. J. Mol. Sci.* **2020**, *21* (3), No. 1131.
(96) Aitha, S.; Thumma, V.; Matta, R.; Ambala, S.; Jyothi, K.; Manda, S.; Pochampally, J. Antioxidant Activity of Novel 4H-Chromene Tethered 1, 2, 3-Triazole Analogues: Synthesis and Molecular Docking Studies. *Results Chem.* **2023**, *5*, No. 100987.
(97) Kotian, S.-Y.; Husain, K.; Rai, K.-L.; Saleh, E.-A.; Hassan, I.; Sabeen, S. Synthesis of 5-{[(1Hbenzo [d] imidazol-2-yl) sulfonyl] methyl}-3-phenyl-4, 5-dihydroisoxazole derivatives, invitro antibacterial and antioxidant studies along with their insilico analyses. *J. Saudi Chem. Soc.* **2023**, *27* (3), No. 101638.

https://doi.org/10.1021/acsomega.3c07555
ACS Omega 2024, 9, 7850−7868